

Applications of symmetry in point-line-plane frameworks for CAD

Patrick W. Fowler

Department of Chemistry, University of Sheffield,
Sheffield S3 7HF, UK

Simon D. Guest

Department of Engineering, University of Cambridge,
Trumpington Street, Cambridge CB2 1PZ, UK

John C. Owen

Siemens, Francis House,
112 Hills Road, Cambridge CB2 1PH, UK

December 9, 2020

Abstract

Computer-aided design (CAD) typically deals with geometries (points, lines and planes) subject to constraints on distances and angles. Simple counting of freedoms and constraints, as used in the analysis of engineering structures, also provides a useful condition on the residual freedoms of a CAD drawing. Here we derive general *symmetry-extended* counting equations to account more fully for the balance of freedoms and constraints in 2D point-line and 3D point-line-plane frameworks. General forms are given for symmetries of the freedoms of points, lines and planes, and constraints based on distances and angles. The resulting toolkit can be used to give stronger conditions on dimensioning of CAD drawings. This importation to CAD of a physical point of view, in which residual freedoms correspond to the mechanisms and redundant constraints to the states of self-stress of a structure composed of bodies and joints, can often reveal hidden freedoms and redundancies in CAD systems. Point-group symmetry is not a panacea: mechanisms that depend on specific geometries may escape detection by symmetry alone. One systematic limitation of

this type is proved for polyhedra with planar faces and prescribed edge lengths.

1 Introduction

Constraint solving is an important aspect of computer-aided design (CAD), and there is a considerable literature that deals with movability of kinematic mechanisms/linkages and geometric constraint solving (Owen, 1991; Bouma et al., 1995; Kim et al., 1998; Barton et al., 2009; Müller, 2016; Sitharam et al., 2019). This paper takes a cross-disciplinary approach to the consideration of systems of points, lines and planes subject to constraints that can be specified in terms of distances and angles. Such configurations give representations of physical systems that may be simple but are sufficient to encompass many engineering structures and mechanisms and they are already versatile enough to allow description of the balance of geometric freedoms and constraints involved in setting up and dimensioning engineering drawings. There is a close analogy between these two types of application. For example, sets of points with distance constraints are precisely analogous to bar-and-joint frameworks in structural engineering. Symmetry analysis of such frameworks, and generalisations to other combinations of bodies and joints have proved fruitful (Fowler and Guest, 2000; Guest and Fowler, 2005; Owen and Power, 2010; Guest et al., 2010). Here we adapt and extend this analysis to the general case of a set of points, lines and planes that is subject to constraints.

The basic objects in the present analysis are *geometries* (points, lines and planes), which are ‘decorated’ as needed with motifs to represent the applicable constraints mathematically in a way that avoids singularities. For example, *signed* distances are used in 2D to give a non-singular description of the point-line distance constraint that continues smoothly to the case when the point lies on the line; in the drawings used in the present paper, this constraint would be represented by decorating the line with a perpendicular displacement arrow. In effect, we are treating lines in 2D and planes in 3D as half-spaces (Jackson and Owen, 2016).

In the spirit of Maxwell counting (Maxwell, 1864; Calladine, 1978) in engineering, for the present application to drawings we first establish the freedoms associated with geometries and the constraints imposed by the various distance and angle conditions. We count these in order to establish the number of residual freedoms in a drawing, which would correspond in the engineering context to the net mobility in a structure. Then we find symmetry extensions to Maxwellian and Calladinean counting rules for systems of points and lines in 2D and of points, lines and planes in 3D. The theory

of group representations when applied to the symmetry-extended freedom count can often detect the presence of redundant constraints and excess freedoms in a drawing, even when this is not detected by the simple freedom count.

Such symmetry techniques have often been used in an engineering context where the requirement is to describe a system that has mobility (Fowler and Guest, 2005). Each application requires some tailoring to the types of object under consideration, whether bars, bodies and joints as in engineering, or geometries and constraints, as here. For applications in CAD, the perspective is further extended, in that we are also interested in finding solutions to the constraint equations (i.e. determining the coordinates of the geometries) for given values for the constraints (such as the distances between pairs of points and lines or the angle between pairs of lines) (Owen, 1991). Typically, we may be given approximate coordinates for the geometries and required to find precise coordinates nearby that satisfy the constraints exactly. A consequence of the inverse function theorem (Spivak, 1965) is that for every excess freedom detected by symmetry there is a corresponding locally redundant constraint, which means it can be removed without affecting the solution space in the neighbourhood of the configuration.

An important property of the constraint equations is that they may be quadratically solvable, by which we mean they can be solved using only the successive solution of quadratic equations, equivalent to the classical notion of constructibility with ruler and compasses (Jackson and Owen, 2019). The fact that some constraints are locally redundant can make it easy to determine that the constraint equations are quadratically solvable and hence to solve them, as we show in examples below.

The plan of the paper is as follows. In §2 the groundwork is laid for the guiding analogy between concepts in CAD and structural engineering, and an example shows the useful role of symmetry in recognition of potential problems with dimensioning of drawings. Counting rules, both scalar and symmetry-extended, are worked out for systems of points, lines and planes (§3). In §4, general expressions for the symmetries of the respective freedoms are obtained (Eqns (4.1) to (4.4), and (4.9)). In §5, symmetries for the various types of distance and angle constraints are tabulated (Figures 3 and 4). As described in §6, this tabulation gives a toolkit for use with the overall mobility equation (6.1) in applications to specific systems. Examples where symmetry-extended equations detect hidden freedoms and redundant constraints in CAD systems are given in §7. There are some systematic limitations on the information that a pure symmetry approach can provide. A general result in §8 shows cancellation of symmetries of freedoms and constraints on geometries in polyhedra with planar faces and fixed edge lengths. A

detailed treatment is given in §9 of freedoms and constraints for the frequently encountered case of the cubic polyhedral cage (3D embedding of a cubic polyhedral graph), of relevance to CAD, structural mechanics, and design of chemical force fields. The paper ends with some brief conclusions.

2 CAD, structural engineering and symmetry

The upper panel of Figure 1 shows two similarly dimensioned drawings, which were created in the commercial design system NX from Siemens. A drawing is said to be *fully dimensioned* if it has enough dimensions and annotations to enable precise replication on a drawing board or in another CAD system. If any small, but non-zero, change to each dimension value in turn (keeping the others unchanged) determines another dimensioned drawing, then the drawing is said to be *independently dimensioned*. A drawing which is both fully and independently dimensioned is said to be *well dimensioned*.

Comparison of the upper and lower drawings in Figure 1(a) shows that they are not fully dimensioned, since the height of the horizontal construction line is different in the two drawings. The reader can easily verify that, for any reasonable positioning of the horizontal construction line, the drawing can be made by ignoring any one of the dimensioned line segments in the left-hand part of the drawing and any one in the right-hand part of the drawing. The drawing can then be constructed sequentially (using only ruler and compasses). On completion, the removed segments will be found to have the required length. This shows that the drawing is neither fully nor independently dimensioned.

The lower panel, Figure 1(b), shows two slightly modified drawings in which the reflection symmetries of the drawing have been broken in distinct ways. In the upper drawing, the overall reflection symmetry is maintained and the internal reflection symmetry within the component pieces is broken. In the lower drawing, the symmetry of the component pieces is maintained but the overall symmetry is broken. The reader is invited to determine which of these, if either, is well dimensioned.

In fact, the upper drawing is well dimensioned whereas the lower drawing is not. The methods to be described in this paper can be used to prove that the lower drawing is neither independently nor fully dimensioned. All variants of the lower drawing can be constructed sequentially with ruler and compasses using the method described above.

The upper drawing is almost certainly not constructible with ruler and

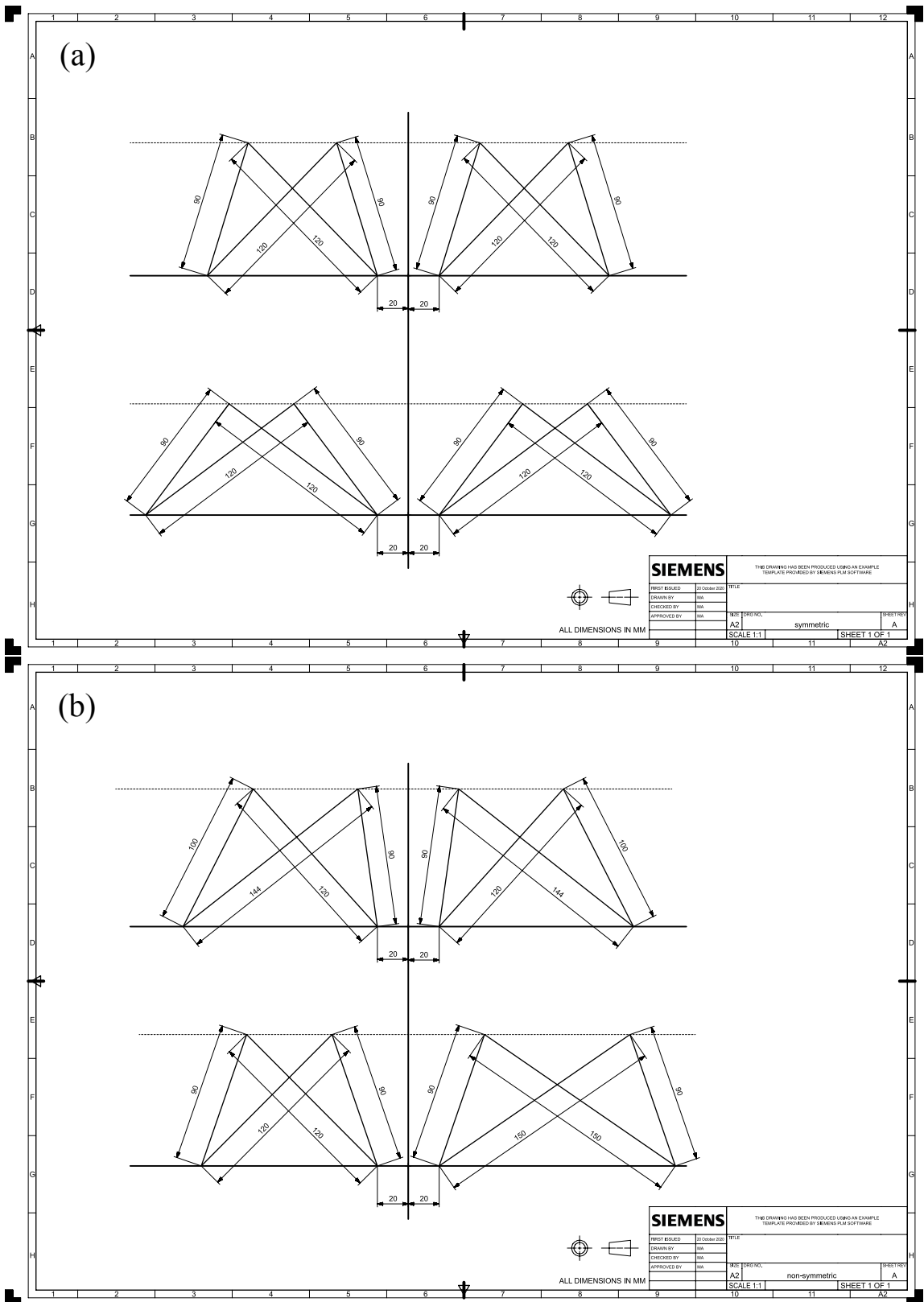


Figure 1: Four CAD drawings of the same basic design with different dimension values. Of these, only the upper drawing of (b) is well dimensioned.

compasses (Owen, 1991) and requires a CAD system that has a numerical constraint solving capability. This drawing was made using the 2D DCM constraint solver, which was developed by one of the authors and colleagues and is incorporated into the NX product from Siemens and into many other commercial CAD products. The fact that the upper drawing is well dimensioned is easily verified in 2D DCM by showing that the Jacobian matrix of the system of constraint equations has independent rows and maximum rank.

The group representation methods used in this paper to determine the balance of freedoms and constraints were first applied in the analysis of the rigidity of structures (Kangwai and Guest, 1999; Guest and Fowler, 2005, 2007). As this field uses terminology rather different from that used in CAD and constraint solving, we will describe the relationship between them with the aid of our example.

From a CAD perspective, the drawing consists of eight line segments (each with a length specified by the dimensions) and one construction line. Four of the line segments have an end point whose coordinates can be specified independently as $(-20, 0)$ and $(20, 0)$ and the other four have an end point which has a zero y -coordinate. A completely free line segment has three freedoms corresponding to rigid body motions. Hence, four of the segments have one freedom and the other four have two freedoms giving a total of twelve freedoms. Two of the segments are automatically connected because their endpoints include a pair with the same coordinates. Connectivity of the ends of other segments, which lie on the x -axis, introduces two constraints and connectivity of the segments at the remaining four points introduces eight further constraints. The construction line ensures that four of the common segment ends are collinear, and since any two points are collinear this introduces two further constraints. There is a total of twelve freedoms and twelve constraints which gives a residual freedom count of zero and suggests that the drawing might be fully dimensioned.

This process of counting freedoms and constraints is automated in dimensional constraint solving software. We describe briefly how this is done in the 2D DCM software component. A line segment is broken into two points and a line. Each point is constrained to be coincident with the line, and the length of the segment is specified by a distance dimension between the two points. Line segments with a common endpoint share the same point. Construction lines are represented as lines and the x - and y -axes are also represented as ‘fixed’ lines. Unfixed points and lines each have two freedoms. Each of the four drawings in Figure 1 has eight points, eleven lines (two of which are fixed), twenty-four point-line coincident constraints, two point-line distance constraints and eight point-point distance constraints. Again, this

gives a residual freedom count of zero.

In structural engineering terms, this design corresponds to a bar-joint framework with two slider joints. Each point corresponds to a joint and each dimension between two points corresponds to a bar. Two of the joints are pinned. The construction line and the x -axis each correspond to a slider joint. Each unpinned joint has two positional freedoms (in 2D) and each bar imposes one constraint. The slider joints each impose two constraints. The net mobility of the structure is zero.

The difference between the number of freedoms and constraints is known as the net mobility of a structure and corresponds to the residual freedoms in a drawing. A drawing is fully dimensioned if the corresponding structure is rigid, and well dimensioned if the corresponding structure is minimally rigid.

The Jacobian matrix in constraint solving is called the rigidity matrix in structural engineering (with each row of the matrix divided by 2). This matrix has a column for each freedom and a row for each constraint. The number of residual freedoms, which corresponds to the net mobility, is the difference between the number of rows and columns.

Vectors in the kernel of the rigidity matrix are called *flexes* (or infinitesimal mechanisms), and vectors in the cokernel are called *self-stresses* (named after the corresponding internal equilibrium forces that can therefore exist). The kernel of the rigidity matrix has a subspace of *internal* flexes which are orthogonal to the infinitesimal rigid body motions. The dimension of the space of self-stresses is denoted by s and that of the space of internal flexes by m . The rigidity matrix determines the first order or infinitesimal rigidity properties of the structure, which is said to be infinitesimally rigid if $m = 0$, and infinitesimally independent if $s = 0$. A basic theorem of linear algebra states that the difference between the numbers of columns and rows of a matrix is equal to the difference between the dimensions of its kernel and cokernel. This is known in structural engineering as the Maxwell/Calladine relation (or counting rule). If $s = 0$, then rigidity and infinitesimal rigidity are equivalent. If $m = 0$, then s gives the number of locally redundant constraints. A structure is called *isostatic* if both $m = 0$ and $s = 0$.

As the examples in Figure 1 show, a drawing may not be well dimensioned even though it has a residual freedom count of zero. This happens for special positions of the geometry. Similar examples are studied in robotics. For example, a Stewart-Gough platform is known to have an ‘internal’ motion if the upper joints lie on a conic and the lower joints also lie on a conic and these two conics are in projective equivalence (Nawratil, 2013). In our case, we use methods from group theory to show that drawings with no residual freedoms may not be well dimensioned, owing to the interplay between symmetry in the dimensioning scheme and symmetry in the positions of the geometries.

This property also leads to redundant dimensions and often allows the simple construction of drawings that would otherwise be difficult without numerical methods.

The essential idea we use is that if a structure or drawing (or part of a drawing or structure) is symmetrical then both the geometries and the constraints can be viewed separately under each symmetry operation (Kangwai and Guest, 1999). A geometry is *unshifted* if its coordinates are left unchanged by the symmetry operation. A pairwise constraint is unshifted if either both geometries connected by the constraint are unshifted, or both are of the same type and their coordinates are exchanged. It is clear from linear algebra that a structure cannot be infinitesimally rigid if a count of the residual freedoms is greater than zero and from the inverse function theorem that it cannot be rigid if in addition it has no states of stress. Similarly, it can be shown that the structure cannot be infinitesimally rigid if a count of the residual freedoms (suitably defined) of only the unshifted geometry and constraints is greater than zero (Owen and Power, 2010). In this case, group representation theory may also imply the symmetry of the flexes and determine whether they preserve the original symmetry of the structure. If the original symmetry is preserved and there are no self-stresses with the same symmetry (or which are fully symmetric), then the structure supports a finite motion (a continuous flex) (Schulze, 2010) and the corresponding dimensioned drawing is not fully dimensioned.

The freedom count that is assigned to a geometry under a symmetry operation is the trace of the transformation matrix which describes the effect of the operation on the geometry coordinates. For example, a point in 2D has zero freedom count under a reflection (which reverses one of a pair of orthogonal translations and preserves the other) whereas it has a count of -2 under a half-turn rotation (which reverses translations in both x - and y - directions). Similarly, the effective number of freedoms removed by a constraint may depend on the type of constraint and the symmetry operation. In the following sections we show how these numbers are computed and provide a complete tabulation for points, lines and planes in 2D and 3D and for various constraints between them.

3 Points, lines and planes

Scalar counting Points in 2D each have two degrees of freedom, and points in 3D have three. Lines in 2D have two degrees of freedom (a translation perpendicular to the line direction and a rotation in the plane). Lines in 3D have four degrees of freedom (translations along, and rotations about, two

independent axes perpendicular to the line). For lines, these freedoms can be considered as the set of all possible rigid-body motions with subtraction (in 2D) of the translation along the line, or (in 3D) of this translation and the rotation about the line. Another justification for the 4-parametric nature of the family of 3D lines is via Plücker coordinates, which are 6-tuples subject to the quadratic constraint known as Klein’s quadric (Plücker, 1865b,a; Klein, 1870).

A plane has three degrees of freedom, which we may consider as one freedom to translate along the normal to the plane and two freedoms to rotate about independent in-plane axes. We may also regard these freedoms as derived from the six freedoms of rigid-body motion by exclusion of the single rotation about the plane normal and the pair of translations orthogonal to the plane normal.

Hence, the Maxwell/Calladine counting rule for the net mobility of a system of points, lines and planes is (in 3D and 2D):

$$3D: \quad m - s = 3P + 4L + 3S - C - 6, \quad (3.1)$$

$$2D: \quad m - s = 2P + 2L - C - 3, \quad (3.2)$$

where P , L and S are the numbers of points, lines and planes, and C is the total number of freedoms removed by constraints. Constraints may be imposed on *distances* (D) of types labelled PP , PL , PS , LL , LS , SS in 3D, or PP , PL , LL in 2D, or on *angles* (A) of types labelled LL , LS , SS in 3D, or LL in 2D. A constraint typically removes a single degree of freedom, but may in some settings remove more. Finally, the constant terms of -6 and -3 on the right-hand sides of (3.1) and (3.2) account for removal of rigid-body motions of the whole system.

The mobility equations (3.1) and (3.2) give the balance $m - s$, but do not determine m and s separately. Further information on m and s may often be obtained by extending pure counting equations such as these to account for *symmetries* of mechanisms and states of self-stress (Fowler and Guest, 2000; Guest and Fowler, 2005).

Symmetry-extended counting In CAD, a constrained system of points, lines and planes is usually described by a graph in which the vertices are labelled with the type of geometry (point, line or plane) that they represent, and likewise the edges are labelled with the type of constraint (distance or angle) that they represent.

A constrained system of points, lines and planes has a point group \mathcal{G} consisting of the symmetry operations that leave the system as a whole

unchanged. The general principle behind the construction of symmetry-extended versions of counting relations of the Maxwell-Calladine type is that all components of an object occur in sets that themselves have well specified behaviour under the symmetries of the object itself. This extends to decorations of the object with sets of scalars, vectors or other local symbols and motifs. Consideration of these symmetries allows construction of a single symmetry-extended counting rule that embodies the ordinary scalar Maxwell/Calladine count as a special case, and in favourable cases adds further conditions on the separate contributions of m and s to the generalised mobility count.

In the present application, the sets of structural components, freedoms and constraints have characters $\chi(g)$ under the various symmetry operations $g \in \mathcal{G}$, which define their (typically reducible) representations Γ . (For definitions and use of terms, see our earlier papers and standard texts (Altmann and Herzig, 1994; Bishop, 1973)). Symmetry operations do not mix geometries or constraints of different types.

An illustration for a simple case is given in Figure 2. The point group considered is C_{2v} , with a list of four symmetry elements, consisting of the identity E ; an axis of two-fold rotation, C_2 ; and two orthogonal mirror planes, σ_1 and σ_2 (Figure 2(a)). The character table (Figure 2(b)) is generated from the group multiplication table by standard methods (see, e.g., (Griffith, 2009)), and here has four irreducible representations, A_1 , A_2 , B_1 and B_2 . Hence, the possible symmetry behaviour of any set of structural components or local motifs of a C_{2v} -symmetric object is described by some linear combination of these. The figure shows the contrasting nodal behaviour of scalar functions of each type (Figure 2(c)), and then illustrates (Figures 2(d)-2(g)) the ways in which they combine to give reducible representations for sets of scalars and vectors associated with vertices and edges of a simple geometrical object in a C_{2v} setting. Representations can be added and multiplied, character by character, according to standard rules (Altmann and Herzig, 1994; Bishop, 1973).

Our aim here is to establish relations between the symmetries of geometries, freedoms and constraints to act as symmetry-extended parallels to the scalar counting rules. A comprehensive list of the various reducible representations needed for this task is calculated in the next two sections.

4 Freedoms

We consider in turn the symmetries of freedoms of points, lines and planes.

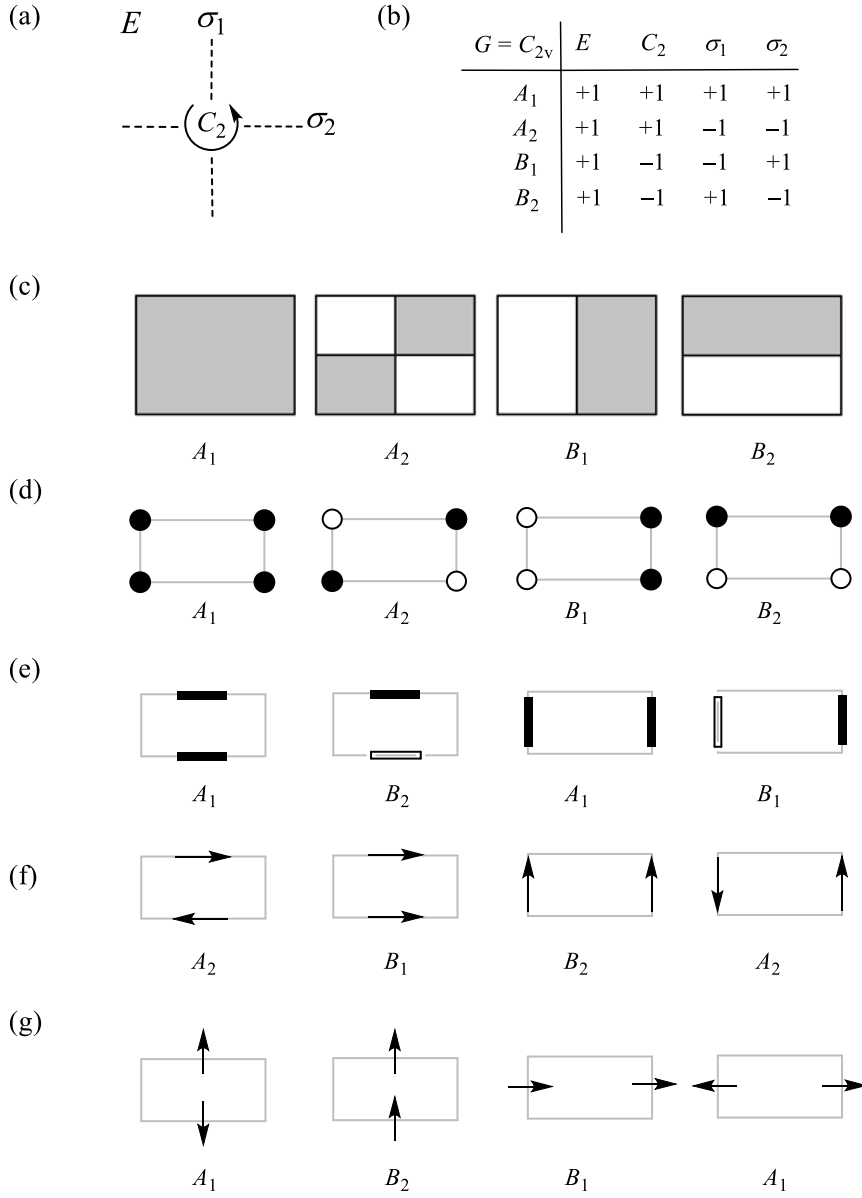


Figure 2: Representations of sets of components and decorations in the point group of an object. (a) Symmetry elements of the C_{2v} point group; (b) Character Table, showing classes of symmetry operations (columns) and the irreducible representations (rows). (c) Symmetry-enforced nodal patterns in scalar functions transforming as each irreducible representation. (d) Permutation representation of the vertices of a rectangle in a C_{2v} setting. The reducible representation is $\{4, 0, 0, 0\}$, where entries give the characters for the four symmetry operations. This reduces to $\Gamma(v) = A_1 + A_2 + B_1 + B_2$. (e) Permutation representation of the edges of the rectangle. $\Gamma(e) = \{4, 0, 2, 2\} = 2A_1 + B_1 + B_2$. (f) Representation of vectors *along* edges of the rectangle. $\Gamma_{\parallel}(e) = \{4, 0, -2, -2\} = 2A_2 + B_1 + B_2$. (g) Representation of vectors *across* edges of the rectangle. $\Gamma_{\perp}(e) = \{4, 0, 2, 2\} = 2A_1 + B_1 + B_2$. Black/white-filled circles/bars in diagrams indicate +1 and -1 local scalars.

Points Following Fowler and Guest (2000), the representation of the freedoms of a set of points is simply

$$3\text{D:} \quad \Gamma_{\text{freedom}}(P) = \Gamma(P) \times \Gamma_{\text{T}}, \quad (4.1)$$

$$2\text{D:} \quad \Gamma_{\text{freedom}}(P) = \Gamma(P) \times \Gamma(T_x, T_y), \quad (4.2)$$

where $\Gamma(P)$ is the permutation representation of the points, with character $\chi_P(g)$ equal to the number of points that are left unshifted by the operation g . Γ_{T} is the representation of the set of translations, $\Gamma_{\text{T}} \equiv \Gamma(T_x, T_y, T_z)$, and $\Gamma(T_x, T_y)$ is its restriction to motion in the x, y plane.

Lines Likewise, the representation of the freedom of the lines is found by direct subtraction to be

$$3\text{D:} \quad \Gamma_{\text{freedom}}(L) = \Gamma(L) \times (\Gamma_{\text{T}} + \Gamma_{\text{R}}) - \Gamma_{\parallel}(L) \times (\Gamma_0 + \Gamma_{\epsilon}), \quad (4.3)$$

$$2\text{D:} \quad \Gamma_{\text{freedom}}(L) = \Gamma(L) \times (\Gamma(T_x, T_y) + \Gamma(R_z)) - \Gamma_{\parallel}(L), \quad (4.4)$$

where $\Gamma_{\text{R}} \equiv \Gamma(R_x, R_y, R_z)$ is the representation of rotations in 3D and $\Gamma(R_z)$ is its restriction to motion in the x, y plane. Also, $\Gamma(L)$ is the permutation representation of the lines and $\Gamma_{\parallel}(L)$ is the representation of a set of vectors directed along the lines, one per line. Γ_0 is the totally symmetric representation ($\chi(g) = +1$ for all g) and Γ_{ϵ} is the antisymmetric representation ($\chi(g) = +1$ for proper g and $\chi(g) = -1$ for improper g). The multiplication of Γ_{\parallel} by Γ_{ϵ} in (4.3) accounts for the pseudo-vector nature of the rotation about the direction of the line.

An equivalent form of $\Gamma_{\text{freedom}}(L)$ that avoids the subtractions in (4.3) and (4.4) is

$$3\text{D:} \quad \Gamma_{\text{freedom}}(L) = \Gamma_{\perp\perp}(L) \times (\Gamma_0 + \Gamma_{\epsilon}), \quad (4.5)$$

$$2\text{D:} \quad \Gamma_{\text{freedom}}(L) = \Gamma(L) \times \Gamma(R_z) + \Gamma_{\perp}(L), \quad (4.6)$$

where (in 3D) $\Gamma_{\perp\perp}(L) = \Gamma(L) \times \Gamma_{\text{T}} - \Gamma_{\parallel}(L)$ is the representation of a set of vectors transverse to the lines, one orthogonal pair per line, or (in 2D) $\Gamma_{\perp}(L)$ is the representation of a set of vectors orthogonal to the lines, one per line. The subscripts \perp and $\perp\perp$ are chosen to reflect the physical distinction in the number of vectors orthogonal to a line in 3D and 2D. The number of freedoms (i.e. the trace of $\Gamma_{\text{freedom}}(L)$ under the identity) is therefore $4L$ in 3D and $2L$ in 2D, as in the scalar relations (3.2) and (3.1).

The forms of equations (4.3) to (4.6) can be justified by considering the transformation properties of the freedoms of a line under operations of the

$\mathcal{G} = D_{\infty h}$	E	$2C_{\infty}(\phi)$	C_2	$\infty\sigma_{\parallel}$	σ_{\perp}	$2S_{\infty}(\phi)$	i	$\infty C'_2$
Γ_T	3	$1 + 2 \cos \phi$	-1	1	1	$-1 + 2 \cos \phi$	-3	-1
$+ \Gamma_R$	3	$1 + 2 \cos \phi$	-1	-1	-1	$1 - 2 \cos \phi$	3	-1
$\times \Gamma(L)$	6	$2 + 4 \cos \phi$	-2	0	0	0	0	-2
	1	1	1	1	1	1	1	1
$- \Gamma_0 \times \Gamma_{\parallel}(L)$	6	$2 + 4 \cos \phi$	-2	0	0	0	0	-2
$- \Gamma_{\epsilon} \times \Gamma_{\parallel}(L)$	-1	-1	-1	-1	1	1	1	1
$= \Gamma_{\text{freedom}}(L)$	4	$4 \cos \phi$	-4	0	0	0	0	0
$\Gamma_0 + \Gamma_{\epsilon}$	2	2	2	0	0	0	0	2
$\times \Gamma_{\perp\perp}(L)$	2	$2 \cos \phi$	-2	0	2	$2 \cos \phi$	-2	0
$= \Gamma_{\text{freedom}}(L)$	4	$4 \cos \phi$	-4	0	0	0	0	0

Table 1: Calculation of $\Gamma_{\text{freedom}}(L)$ for a single line L in 3D. Operations σ_{\parallel} and σ_{\perp} are, respectively, a reflection in any mirror plane containing L and a reflection in the mirror plane normal to L . The operation $C_{\infty}(\phi)$ ($S_{\infty}(\phi)$) is a proper (improper) rotation by ϕ about L , and C'_2 is a 2-fold rotation about any axis perpendicular to L . The special cases of proper and improper rotations associated with the principal axis (i.e. C_2 , σ_{\perp} and i) are listed separately, as they fall into classes of size one. The table reports the calculation according to (4.3), and the check that (4.5) gives the same result.

maximum possible site symmetry group (the group \mathcal{G} of operations that leaves the line in place). These calculations are shown in Tables 1 and 2 for the simplest case of the single line, where \mathcal{G} is $D_{\infty h}$ in 3D and C_{2v} in 2D, and the permutation representation $\Gamma(L)$ is by definition Γ_0 . Reduction of $\Gamma_{\text{freedom}}(L)$ gives $E_{1g} + E_{1u} \equiv \Pi_g + \Pi_u$ ($D_{\infty h}$, 3D) and $A_2 + B_2$ (C_{2v} , 2D) which are respectively the symmetries of translations along and rotations about the two directions orthogonal to the line (in 3D), and the symmetries of the in-plane rotation and the translation perpendicular to the line (in 2D).

Planes It is straightforward to include planes within the symmetry formalism. Let the permutation representation of the set of planes be $\Gamma(S)$. Define $\Gamma_{\perp}(S)$ as the representation of a set of vectors, one along the normal for each plane, and $\Gamma_{\odot}(S)$ as the representation of a set of circular arrows, one around each plane normal. The freedoms of the set of planes span

$$3\text{D:} \quad \Gamma_{\text{freedom}}(S) = \Gamma_{\perp}(S) + \Gamma(S) \times \Gamma_R - \Gamma_{\odot}(S), \quad (4.7)$$

$\mathcal{G} = C_{2v}$	E	C_2	$\sigma_{\parallel} \equiv \sigma_1$	$\sigma_{\perp} \equiv \sigma_2$
$\Gamma(T_x, T_y)$	2	-2	0	0
$+ \Gamma(R_z)$	1	1	-1	-1
	3	-1	-1	-1
$\times \Gamma(L)$	1	1	1	1
	3	-1	-1	-1
$- \Gamma_{\parallel}(L)$	-1	1	-1	1
$= \Gamma_{\text{freedom}}(L)$	2	0	-2	0
	1	-1	-1	1
$+ \Gamma(L) \times \Gamma(R_z)$	1	1	-1	-1
$= \Gamma_{\text{freedom}}(L)$	2	0	-2	0

Table 2: Calculation of $\Gamma_{\text{freedom}}(L)$ for a single line L in 2D. Operations σ_{\parallel} and σ_{\perp} are respectively reflections in L and in the normal to L . The table reports the calculation according to (4.4), and the check that (4.6) gives an identical result.

$\mathcal{G} = D_{\infty h}$	E	$2C_{\infty}(\phi)$	C_2	$\infty\sigma_{\parallel}$	σ_{\perp}	$2S_{\infty}(\phi)$	i	$\infty C'_2$
Γ_{R}	3	$1 + 2 \cos \phi$	-1	-1	-1	$1 - 2 \cos \phi$	3	-1
$+ \Gamma_{\perp}$	1	1	1	1	-1	-1	-1	-1
$- \Gamma_{\odot}$	-1	-1	-1	1	-1	-1	-1	1
	3	$1 + 2 \cos \phi$	-1	1	-3	$-1 - 2 \cos \phi$	1	-1
$\times \Gamma(S)$	1	1	1	1	1	1	1	1
$= \Gamma_{\text{freedom}}(S)$	3	$1 + 2 \cos \phi$	-1	1	-3	$-1 - 2 \cos \phi$	1	1

Table 3: Calculation of $\Gamma_{\text{freedom}}(S)$ for a single plane S . Operations are as defined in Table 1 but now the principal axis lies along the normal to the plane.

where the first term on the RHS represents the translational freedoms along the normal, and the remainder represents the pairs of rotational freedoms. Taking advantage of the fact that the characters $\Gamma_{\perp}(S)$ and $\Gamma_{\odot}(S)$ are identical under proper operations but of opposite sign under improper operations, we can write

$$\text{3D:} \quad \Gamma_{\odot}(S) = \Gamma_{\perp}(S) \times \Gamma_{\epsilon}, \quad (4.8)$$

and hence

$$\text{3D:} \quad \Gamma_{\text{freedom}}(S) = \Gamma(S) \times \Gamma_{\text{R}} + \Gamma_{\perp}(S) \times (\Gamma_0 - \Gamma_{\epsilon}). \quad (4.9)$$

Table 3 gives the calculation for the maximum $D_{\infty h}$ symmetry, where $\Gamma_{\text{freedom}}(S)$ for a single plane spans $A_{1u} + E_{1g} \equiv \Sigma_u^+ + \Pi_g$.

Note that, in the purely rotational point groups that apply to chiral configurations, $\Gamma_{\epsilon} = \Gamma_0$ and $\Gamma_{\text{R}} = \Gamma_{\text{T}}$, so that the representation of plane freedoms reduces in these groups to

$$\text{3D chiral:} \quad \Gamma_{\text{freedom}}(S) = \Gamma(S) \times \Gamma_{\text{T}}. \quad (4.10)$$

In a case where the planes define faces of a polyhedron, we have $\Gamma_{\perp}(S) = \Gamma(S)$ and, on invoking the spherical-shell decomposition into radial and tangential vector components of the product of a permutation representation and the translational representation (Quinn et al., 1984; Fowler and Quinn, 1986), (4.9) reduces to

$$\begin{aligned} \Gamma_{\text{freedom}}(S) &= \Gamma(S) \times \Gamma_{\text{R}} - \Gamma_{\perp}(S) \times \Gamma_{\epsilon} + \Gamma(S) \\ \text{polyhedron:} \quad &= [\Gamma(S) \times \Gamma_{\text{T}} - \Gamma(S)] \times \Gamma_{\epsilon} + \Gamma(S) \\ &= \Gamma_{\pi}(S) \times \Gamma_{\epsilon} + \Gamma(S) \\ &= \Gamma(S) \times \Gamma_{\text{T}}. \end{aligned} \quad (4.11)$$

for any polyhedron, chiral or not. The final step follows from the invariance property of the π representation ($\Gamma_{\pi} \times \Gamma_{\epsilon} = \Gamma_{\pi}$). We will exploit (4.10) in an example later.

5 Constraints

Representations of the constraints are also straightforwardly derived, even if not always easy to describe compactly. In this section, we consider the representation of individual constraints in their maximum site symmetry. In the examples considered in later sections, site symmetries are typically

lowered, and the representations appearing in our equations will be used with descent in symmetry to describe orbits of constraints of a given type.

A note on special configurations that we exclude from consideration: as a pragmatic decision, we rule out distance constraints between pairs of coincident points, lines or planes, because this would cause difficulties with constraints that do not have a finite derivative at distance zero. We do, however, allow parallel constraints between geometrically coincident lines or planes, although care must then be taken about how the actions of symmetry operations are defined (Schulze, 2010). We take the actions at coincidence to be the limit of the actions at small distance.

5.1 Constraints in 2D

We first consider the 2D case. In 2D, we have points and lines, and constraints are of four basic types: (i) distances between points; (ii) distances between points and lines; (iii) distances between lines; (iv) angles between lines. Each type of constraint is illustrated in Figure 3 by the set of motions that it forbids, along with a table describing the character of the constraint under the symmetry operations that leave unshifted the points and lines involved.

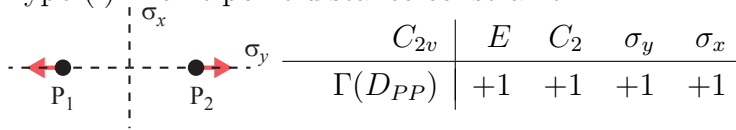
A constraint of type (i) prevents changes in a pairwise distance between two points. As a scalar quantity, it transforms as a bar. The reducible representation spanned by all constraints of type D_{PP} is therefore the permutation representation of a set of notional bars. With our definition, we are implicitly excluding bars of zero length associated with coincidence of points.

A constraint of type (ii) prevents change in the signed perpendicular distance from a line to a point and transforms as a vector perpendicular to the line. The reducible representation spanned by constraints of type D_{PL} is that of the set of such vectors for line-point pairs. We use the *signed* distance because it behaves linearly even in the limit where the point lies on the line. In 2D the constraint has the same dimension whether P is on or off the line L ; this is no longer true in 3D.

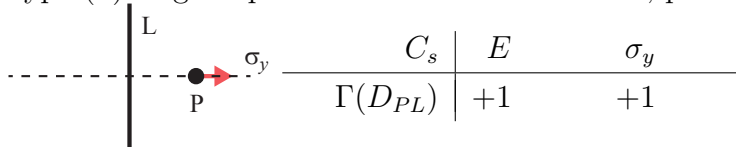
A constraint of type (iii) prevents change in the pairwise distance between two lines, and in 2D is relevant only when the lines have already been constrained to be parallel (by an angular constraint $A_{LL\parallel}$). The additional distance constraint transforms as a bar. The reducible representation of a set of such constraints is the permutation representation of a set of notional bars.

A constraint of type (iv) prevents infinitesimal rotations between the two lines. We distinguish between cases where the lines meet, and where the lines are parallel. The representation for the full set of type (iv) constraints contains contributions from all those of types A_{LL} and $A_{LL\parallel}$.

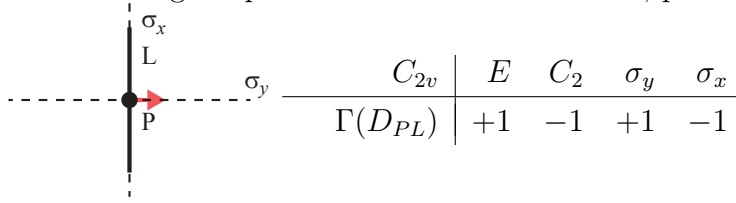
Type (i): Point-point distance constraint



Type (ii): Signed point-line distance constraint, point off the line



Signed point-line distance constraint, point on the line



Type (iii): Line-line distance constraint, lines parallel and non-coincident

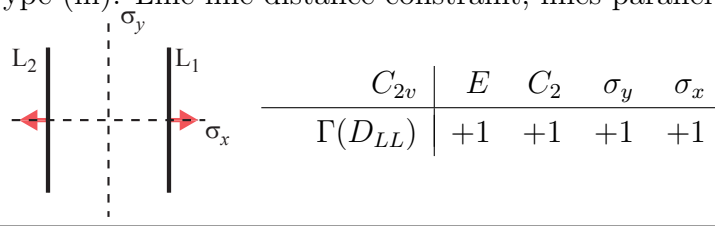
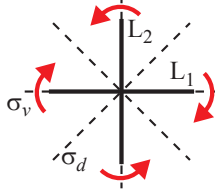


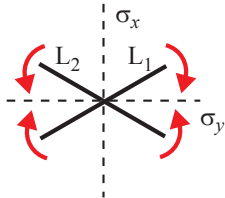
Figure 3: Constraints in 2D, continued overleaf

Type (iv): Line-line angle constraint, perpendicular lines



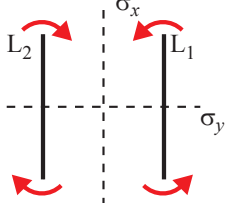
C_{4v}	E	$2C_4$	C_2	$2\sigma_v$	$2\sigma_d$
$\Gamma(A_{LL})$	+1	-1	+1	-1	+1

Line-line angle constraint, general position



C_{2v}	E	C_2	$\overbrace{\sigma_y \quad \sigma_x}$	
$\Gamma(A_{LL})$	+1	+1	+1	+1

Line-line angle constraint, parallel lines



C_{2v}	E	C_2	$\overbrace{\sigma_y \quad \sigma_x}$	
$\Gamma(A_{LL\parallel})$	+1	-1	-1	+1

Figure 3: Contribution to the constraint representation for single constraints of types (i)–(iv) in 2D. Arrows indicate the displacements away from the constrained geometry that are forbidden by the constraint. In each case the maximum site symmetry is shown. To maintain compatibility between 2D and 3D notation, mirror lines are labelled σ_α , indicating that they have their normal along the α -axis.

5.2 Constraints in 3D

Similar reasoning applies to the symmetry description of the constraints in 3D. In 3D the types are (i) to (iv), plus those involving (v) distance of a point to a plane, (vi) distance of a line to a plane, (vii) distance between planes, (viii) angle between a line and a plane, and (ix) angle between two planes. Each type of constraint is illustrated in Figure 4 by the set of motions that it forbids, along with a table describing the character of the constraint in maximum possible local site symmetry.

In 3D, the constraint of type (i) is exactly as described in 2D, and again contributes to the permutation representation of the set of notional bars connecting constrained pairs.

In 3D, for constraints of type (ii) we distinguish two cases. If the point P is not on the line L , the constraint removes one freedom and transforms as a vector along the perpendicular from L to P , which is totally symmetric in the site group. If P lies on L , however, the constraint removes *two* freedoms and transforms as a pair of orthogonal vectors perpendicular to L . Similar doubling up at coincidence applies to line-plane (vii) and plane-plane angle (viii) constraints.

In 3D, for constraints of type (iii) we distinguish between lines that are parallel and lines that are not. If the lines are not parallel, the constraint is of dimension one, preventing changes in the pairwise distance between the lines, and transforms as a bar along the mutual perpendicular. The direction of the perpendicular remains defined even when the distance between the lines tends to zero, but we note that the case of intersecting lines does require more careful treatment. In that case, we are effectively considering the symmetry of a system of two lines, and their corresponding displacement vectors which point in opposite directions along the perpendicular. New symmetry operations that appear in the limit of zero separation may or may not exchange lines *together* with their displacements, and may or may not reverse the directions of those displacements. The combined effect leads to the characters seen in the tables.

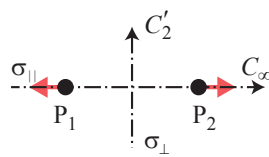
For type (iii) where the lines are already constrained to be parallel, the distance constraint is of dimension one. We are implicitly excluding the case where the distance between two parallel lines is constrained to zero: in this case, the lines would become identical and a distance constraint of dimension two would be required.

In 3D, for constraints of type (iv) there is also a distinction between parallel and non-parallel cases. For non-parallel lines there is a unique definition of the angle between lines defined in the plane normal to the mutual perpendicular, and the symmetry analysis follows a similar course to the

2D case. For constrained systems of type (iv), where the lines are parallel, the constraint is of dimension two. The two lines define a plane (as we are not considering coincident lines), and both in-plane and out-of-plane angular constraints apply.

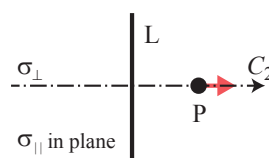
For types (iii) and (iv) the characters for the case of non-zero separation can be derived by elimination of symmetry operations (descent in symmetry). For type (iii) the operations that disappear at finite separation are all those with character -1 in the higher symmetry group; the displacement that increases the separation from zero is fully symmetric in the lower group. For type (iv) this is not the case: some of the symmetry operations that are retained have character -1 ; this is because the motion associated with separation is not the angular freedom that is forbidden by the constraint. Similar considerations apply to the constraints (v) to (viii) that involve planes.

Type (i): Point-point distance constraint



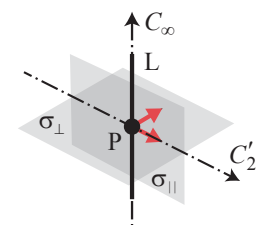
$D_{\infty h}$	E	$2C_{\infty}(\phi)$	C_2	$\infty\sigma_{\parallel}$	σ_{\perp}	$2S_{\infty}(\phi)$	i	$\infty C_2'$
$\Gamma(D_{PP})$	+1	+1	+1	+1	+1	+1	+1	+1

Type (ii): Point-line distance constraint, point off the line



C_{2v}	E	C_2	σ_{\parallel}	σ_{\perp}
$\Gamma(D_{PL})$	+1	+1	+1	+1

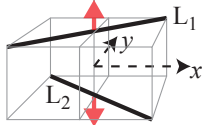
Point-line distance constraint, point on the line



$D_{\infty h}$	E	$2C_{\infty}(\phi)$	C_2	$\infty\sigma_{\parallel}$	σ_{\perp}	$2S_{\infty}(\phi)$	i	$\infty C_2'$
$\Gamma(D_{PL0})$	+2	$2 \cos \phi$	-2	0	+2	$2 \cos \phi$	-2	0

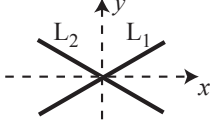
Figure 4: Constraints in 3D, continued overleaf

Type (iii): Line-line distance constraint, lines in general position



Distance non-zero

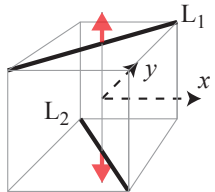
D_2	E	C_{2z}	C_{2x}	C_{2y}
$\Gamma(D_{LL})$	+1	+1	+1	+1



Distance zero

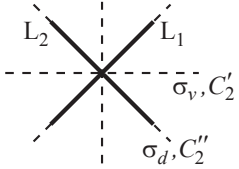
D_{2h}	E	C_{2z}	C_{2x}	C_{2y}	i	σ_z	σ_x	σ_y
$\Gamma(D_{LL})$	+1	+1	+1	+1	-1	-1	-1	-1

Line-line distance constraint, lines perpendicular



Distance non-zero

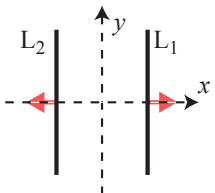
D_{2d}	E	C_2	$2C'_2$	$2S_4$	$2\sigma_d$
$\Gamma(D_{LL})$	+1	+1	+1	+1	+1



Distance zero

D_{4h}	E	$2C_4$	C_2	$2C'_2$	$2C''_2$	i	$2S_4$	σ_h	$2\sigma_v$	$2\sigma_d$
$\Gamma(D_{LL})$	+1	-1	+1	+1	-1	-1	+1	-1	-1	+1

Line-line distance constraint, lines parallel



D_{2h}	E	C_{2z}	C_{2x}	C_{2y}	i	σ_z	σ_x	σ_y
$\Gamma(D_{LL\parallel})$	+1	+1	+1	+1	+1	+1	+1	+1

Figure 4: Constraints in 3D, continued overleaf

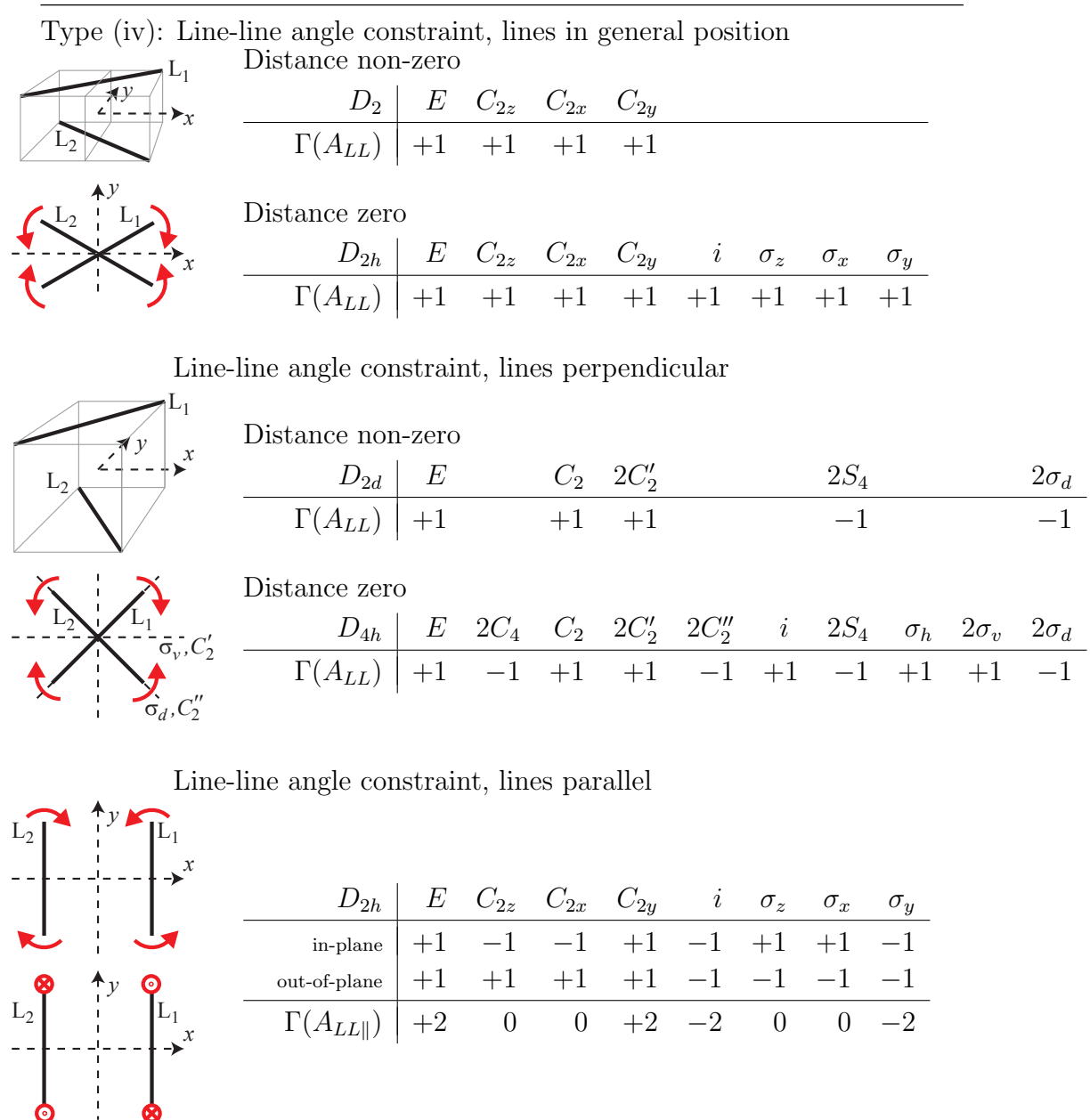
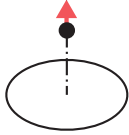


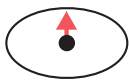
Figure 4: Constraints in 3D, continued overleaf

Type (v): Point-plane distance constraint, point off plane



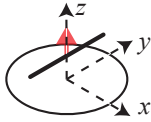
$C_{\infty v}$	E	$2C_{\infty}(\phi)$	C_2	$\infty\sigma_v$
$\Gamma(D_{PS})$	+1	+1	+1	+1

Point-plane distance constraint, point in plane



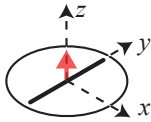
$D_{\infty h}$	E	$2C_{\infty}(\phi)$	C_2	$\infty\sigma_v$	σ_h	$2S_{\infty}(\phi)$	i	$\infty C'_2$
$\Gamma(D_{PS})$	+1	+1	+1	+1	-1	-1	-1	-1

Type (vi): Line-plane distance constraint, line off the plane



C_{2v}	E	C_{2z}	σ_x	σ_y
$\Gamma(D_{LS})$	+1	+1	+1	+1

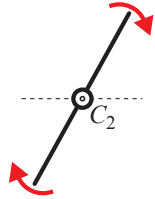
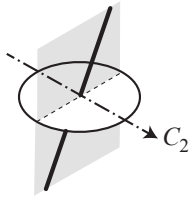
Line-plane distance constraint, line on the plane



D_{2h}	E	C_{2z}	C_{2x}	C_{2y}	i	σ_z	σ_x	σ_y
$\Gamma(D_{LS})$	+1	+1	-1	-1	-1	-1	+1	+1

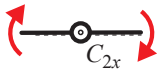
Figure 4: Constraints in 3D, continued overleaf

Type (vii): Line-plane angle constraint, general position



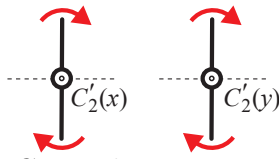
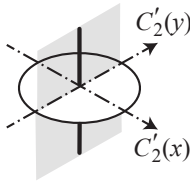
C_{2h}	E	C_{2x}	i	σ_h
$\Gamma(A_{LS})$	+1	+1	+1	+1

Line-plane angle constraint, line in plane



D_{2h}	E	C_{2z}	C_{2x}	C_{2y}	i	σ_z	σ_x	σ_y
$\Gamma(A_{LS})$	+1	-1	+1	-1	+1	-1	+1	-1

Line-plane angle constraint, line normal to plane



General setting:

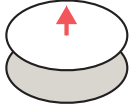
$D_{\infty h}$	E	$2C_{\infty}(\phi)$	C_2	$\infty\sigma_v$	σ_h	$2S_{\infty}(\phi)$	i	$\infty C'_2$
$\Gamma(A_{LS\perp})$	+2	$2\cos(\phi)$	-2	0	-2	$-2\cos\phi$	+2	0

Orthorhombic subgroup

D_{2h}	E	C_{2z}	C_{2x}	C_{2y}	i	σ_z	σ_x	σ_y
yz -plane	+1	-1	+1	-1	+1	-1	+1	-1
xz -plane	+1	-1	-1	+1	+1	-1	-1	+1
$\Gamma(A_{LS\perp})$	+2	-2	0	0	+2	-2	0	0

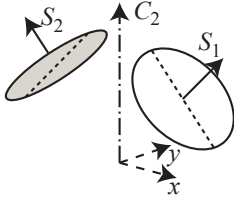
Figure 4: Constraints in 3D, continued overleaf

Type (viii): Plane-plane distance constraint



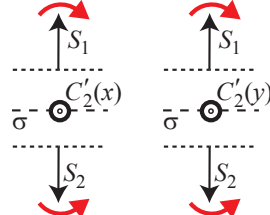
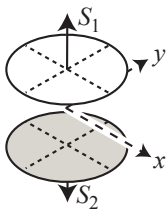
$D_{\infty h}$	E	$2C_{\infty}(\phi)$	C_2	$\infty\sigma_h$	σ_h	$2S_{\infty}(\phi)$	i	$\infty C'_2$
$\Gamma(D_{SS})$	+1	+1	+1	+1	+1	+1	+1	+1

Type (ix): Plane-plane angle constraint, general position



D_{2h}	\vec{E}	C_{2z}	C_{2x}	C_{2y}	i	σ_z	σ_x	σ_y
$\Gamma(A_{SS})$	+1	-1	+1	-1	+1	-1	+1	-1

Plane-plane angle constraint, planes parallel



General setting:

$D_{\infty h}$	E	$2C_{\infty}(\phi)$	C_2	$\infty\sigma_v$	σ_h	$2S_{\infty}(\phi)$	i	$\infty C'_2$
$\Gamma(A_{SS\parallel})$	+2	$2 \cos(\phi)$	-2	0	+2	$2 \cos \phi$	-2	0

Orthorhombic subgroup

D_{2h}	E	C_{2z}	C_{2x}	C_{2y}	i	σ_z	σ_x	σ_y
yz -plane	+1	-1	-1	+1	-1	+1	+1	-1
xz -plane	+1	-1	+1	-1	-1	+1	-1	+1
$\Gamma(A_{SS\parallel})$	+2	-2	0	0	-2	+2	0	0

Figure 4: Contribution to the constraint representation for single constraints of type (i)–(ix) in 3D. Arrows indicate the displacements away from the constrained geometry that are forbidden by the constraint. In each case the maximum possible site symmetry is shown. Particular settings for the reduction $D_{\infty h} \rightarrow D_{2h}$ are given for types (vii) and (ix).

6 Net mobility

Collection of the partial results gives the total representation of the balance of freedoms and constraints. The final form of this representation is

$$\Gamma(m) - \Gamma(s) = \Gamma_{\text{freedom}} - \Gamma_{\text{constraint}} - \Gamma_{\text{rigid}}, \quad (6.1)$$

where Γ_{freedom} is defined by the sum of representations of point, line and plane freedoms, $\Gamma_{\text{constraint}}$ is defined by the sum over constraints of the representations of the freedoms removed by each type: $\Gamma(D_{PP})$, $\Gamma(D_{PL})$, $\Gamma(D_{PL0})$, $\Gamma(D_{PS})$, $\Gamma(D_{LL})$, $\Gamma(D_{LL\parallel})$, $\Gamma(D_{LS})$, $\Gamma(D_{SS\parallel})$ for distances, and $\Gamma(A_{LL})$, $\Gamma(A_{LL\parallel})$, $\Gamma(A_{LS})$, $\Gamma(A_{LS\perp})$, $\Gamma(A_{SS})$, $\Gamma(A_{SS\parallel})$ for angles. The constant representation, Γ_{rigid} , is the representation of rigid-body motions in the space of the appropriate dimension. This general equation can now be applied to any particular case, using the once-and-for-all tables for freedoms and constraints, as derived in §4 and §5.

7 Examples

We now consider some examples from 2D and 3D where symmetry yields extra information, and some telling examples where it does not.

7.1 2D

Constrained crossing four-bar linkage We begin with a 2D example based on the well known four-bar linkage, expressed as a CAD problem. The relevant point-line system of geometries consists of four points P_1 to P_4 connected in a cycle by four distances of type D_{PP} corresponding to the four bars of the linkage. Two lines L_1 and L_2 are each constrained to pass through a pair of antipodal points by four constraints of type D_{PL} . L_1 and L_2 are constrained to have a fixed relative angle with an angle constraint of type A_{LL} . This classic linkage is generically isostatic.

In the high-symmetry special configuration shown in Figure 5(a), where the set of points, lines and constraints has C_{2v} symmetry (the point group consisting of the identity, a C_2 rotation and a pair of orthogonal mirror planes). The number of constraints and freedoms is the same as in the previous example, but the linkage has a mechanism that is revealed when the symmetry-extended counting rule (3.2) is applied.

As shown in Figure 5(b), the underlying graph of geometries and constraints is a weighted complete bipartite graph $K_{3,3}$, where vertices are points P or lines L , and edges correspond to distance and angle constraints. If

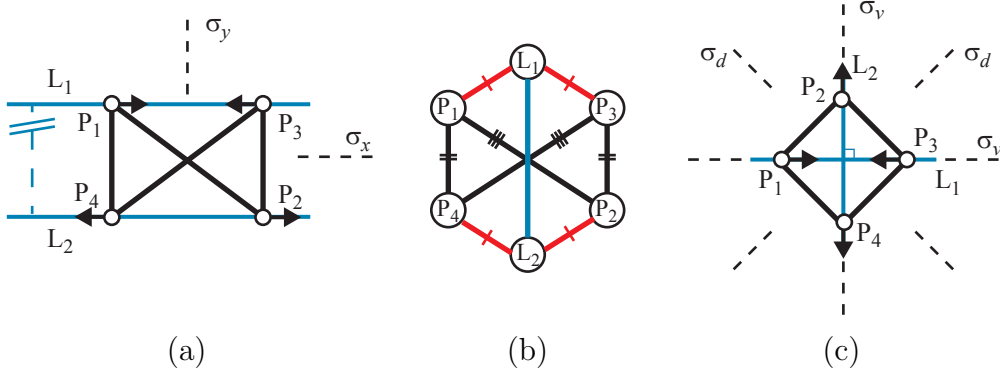


Figure 5: Constrained four-bar linkages. (a) Crossing (C_{2v}) configuration, with points constrained to lie on parallel lines. (b) Corresponding graph of geometries and constraints (D_{PP} in black, D_{PL} in red, A_{LL} in blue, with tick marks indicating equalities). (c) Non-crossing (C_{4v}) configuration, with points arranged as a quadrilateral with diagonals constrained to be perpendicular. The arrows show the initial infinitesimal displacements associated with each finite mechanism.

points, lines, point-point and point-line distance constraints, and line-line angular constraints are respectively counted by P , L , D_{PP} , D_{PL} and A_{LL} , the number of freedoms is $F = 2P + 2L = 8 + 4 = 12$, and the number of constraints is $C = D_{PP} + D_{PL} + A_{LL} = 4 + 4 + 1 = 9$, and hence the mobility count is the isostatic value: $m - s = F - C - 3 = 12 - 9 - 3 = 0$.

Considering the symmetry-extended rule (6.1) for 2D point-line systems, the three constraint types have the following characters under the symmetry operations of C_{2v} :

$\mathcal{G} = C_{2v}$	E	C_2	σ_y	σ_x	Representation
$\Gamma(D_{PP})$	4	2	0	2	$2A_1 + A_2 + B_2$
$\Gamma(D_{PL})$	4	0	0	0	$A_1 + A_2 + B_1 + B_2$
$\Gamma(A_{LL\parallel})$	1	-1	-1	1	B_2

The irreducible representations in the final column of this table can be obtained from standard tables for representations in C_{2v} (Atkins et al., 1970). Summing the representations for the three constraint types,

$$\Gamma_{\text{constraint}} = 3A_1 + 2A_2 + B_1 + 3B_2. \quad (7.1)$$

The freedoms of the points and lines (calculated from (4.2) and (4.4)) span

$$\Gamma_{\text{freedom}} = 3A_1 + 3A_2 + 3B_1 + 3B_2 = 3\Gamma_{\text{reg}}, \quad (7.2)$$

where Γ_{reg} is the regular representation of C_{2v} (with character $\chi(E) = |G|$ and $\chi(g) = 0$ otherwise). Hence, with $\Gamma_{\text{rigid}} = A_2 + B_1 + B_2$,

$$\Gamma(m) - \Gamma(s) = B_1 - B_2, \quad (7.3)$$

revealing a mechanism of B_1 symmetry, which is balanced and cancelled out in the scalar count by a state of self stress of B_2 symmetry. The mechanism preserves σ_y but destroys σ_x , so that the initial C_{2v} point group descends to C_s , in which $\Gamma(m)$ is A' and $\Gamma(s)$ is A'' , in the infinitesimally distorted configuration. As the representations $\Gamma(m)$ and $\Gamma(s)$ do not share a symmetry ($A' \neq A''$), the mechanism is not blocked by the state of self-stress; the initial symmetric configuration is therefore free to distort under the specified constraints. The state of self-stress detected by symmetry corresponds to the forbidden simultaneous lengthening and shortening of the bars P_1P_4 and P_2P_3 . Numerical computation of the rank of the Jacobian matrix of the corresponding system of constraint equations shows that this is the only state of stress and hence that the mechanism is finite (Kangwai and Guest, 1999; Guest and Fowler, 2007).

If the angular constraint between the lines is removed, the B_2 self-stress is eliminated, leaving the B_1 mechanism unchanged. This shows that the angular constraint is locally redundant. The 2D DCM constraint solver which is described in in §2 can be used to exhibit the path of this finite mechanism by replacing this angular constraint with a distance constraint between P_1 and P_3 . The constraint graph is no longer 3-connected and hence is quadratically solvable (Owen, 1991; Owen and Power, 2006). The constraint equations are easily solved for a sequence of small changes in the value for the new distance constraint to obtain a sequence of non-congruent configurations which satisfy all of the original constraints (including the locally redundant angular constraint). A similar method can be used to exhibit all of the finite mechanisms found in other examples in this paper.

If we were to add an extra constraint $D_{LL\parallel}$ on the separation of the parallel lines, $\Gamma_{\text{constraint}}$ would contain an additional A_1 term, indicating the presence of an extra state of self-stress of A_1 symmetry. On descent to C_s , $\Gamma(m) - \Gamma(s)$ would reduce to $-A''$, indicating that the A' mechanism has become symmetry undetectable. The mechanism detected at the high-symmetry point is now infinitesimal, blocked by a fully symmetric state of self-stress in which the vertical bars P_1P_4 and P_2P_3 are in an equal state of tension that is balanced by the compression carried by the $D_{LL\parallel}$ constraint.

Dimensioning: This example also explains why each of the drawings in Figure 1(a) has a redundant dimension. If we add a parallel constraint between the x -axis and the horizontal construction line both the left and right

sub-diagrams are isomorphic to Figure 5(a). This shows that they both induce the parallel constraint and that without the additional constraint any one of the distant dimensions in the sub-diagrams is redundant. This argument does not require a symmetry between the left and right sub-diagrams which explains why the lower drawing in Figure 1(b) also has a redundant dimension. The corresponding sub-diagrams in the upper drawing of Figure 1(b) have no symmetry but the whole drawing has C_s reflection symmetry about the y -axis. We now show that the overall C_s symmetry alone does not predict that the drawing is not well dimensioned.

We use the procedure for counting residual freedoms that is used by 2D DCM, described in Section 2. The geometry comprises eight points and eleven lines. Two of the lines correspond to the x - and y axes and one corresponds to the construction line. These lines are all unshifted by the reflection symmetry. The remaining eight lines that correspond to the displayed line segments, and all the points, are moved by the reflection. There are twenty four point-line coincident constraints and two point-line distance dimensions which are all type D_{PL} and eight point-point distance dimensions which are all type D_{PP} . These are all moved by the reflection. There is also a perpendicular constraint, type A_{LL} , between the lines which correspond to the x - and y axes. This constraint is unshifted by the reflection symmetry. The character table below shows the full cancellation of the characters for the identity and the reflection operations.

$\mathcal{G} = C_s$	E	σ	Representation
$-\Gamma(D_{PP})$	-8	0	$-4A - 4A'$
$-\Gamma(D_{PL})$	-26	0	$-13A - 13A'$
$-\Gamma(A_{LL})$	-1	1	$-A'$
$-\Gamma_{\text{constraint}}$	-35	1	$-17A - 18A'$
$-\Gamma_{\text{T}} - \Gamma_{\text{R}}$	-3	1	$-A - 2A'$
$-\Gamma(P)$	16	0	$8A + 8A'$
$-\Gamma(L)$	22	-2	$-10A + 12A'$
$-\Gamma_{\text{freedom}}$	38	-2	$18A + 20A'$
$\Gamma(m) - \Gamma(s)$	0	0	\emptyset

This complete cancellation implies that there is no reason arising from the overall reflection symmetry for the design not to be well dimensioned. Numerical calculation of the Jacobian matrix of the constraint equations in 2D DCM shows, as expected, that $m = 0$ and $s = 0$ for the configuration shown in the upper panel of Figure 1(b), but $m = 1$ and $s = 1$ for the other three configurations.

Non-crossing four-bar linkage Figure 5(c) shows an alternative configuration for the four-bar linkage, in which the bars do not cross but instead form the four sides of a quadrilateral. The two lines are diagonals of the quadrilateral and are connected by an angular constraint. This linkage is generically isostatic.

In the high-symmetry special configuration shown in the figure, where the four points are on the corners of a square, the sets of points, lines and constraints has C_{4v} symmetry where the two mirror planes σ_v each contain one of the lines. The corresponding graph of geometries and constraints is still $K_{3,3}$, as for the parallel-constrained linkage (Figure 5(b)), but now tick-marked to indicate equality of all four black edges. The number of freedoms and constraints is the same as in the previous example.

In this configuration the three constraint types have the following characters under the symmetry operations of C_{4v} :

$\mathcal{G} = C_{4v}$	E	$2C_4$	C_2	$2\sigma_v$	$2\sigma_d$	Representation
$\Gamma(D_{PP})$	4	0	0	0	2	$A_1 + B_2 + E$
$\Gamma(D_{PL})$	4	0	0	-2	0	$A_2 + B_2 + E$
$\Gamma(A_{LL})$	1	-1	1	-1	1	B_2

Summing the representations for the three constraint types gives

$$\Gamma_{\text{constraint}} = A_1 + A_2 + 3B_2 + 2E. \quad (7.4)$$

The freedoms of the points and lines span $A_1 + A_2 + B_1 + B_2 + 2E$ and $A_2 + B_2 + E$, respectively. Hence,

$$\Gamma_{\text{freedom}} = A_1 + 2A_2 + B_1 + 2B_2 + 3E, \quad (7.5)$$

and, with $\Gamma_{\text{rigid}} = A_2 + E$, the net mobility is

$$\Gamma(m) - \Gamma(s) = B_1 - B_2, \quad (7.6)$$

revealing a mechanism of B_1 symmetry, balanced in the scalar count by a state of self stress of B_2 symmetry. The mechanism is not blocked by the state of self-stress and is finite. Removal of the A_{LL} constraint has eliminated the B_2 self-stress without affecting the mechanism with B_1 symmetry. Hence the angular constraint is locally redundant, which also follows from the well known theorem in geometry that the two diagonals of a square are perpendicular. Deletion of this constraint means that the constraint graph is no longer 3-connected and the constraint equations are then recognised as quadratically solvable.

From the entries for B_1 in the character table (with $\chi(C_4) = -1$, $\chi(\sigma_d) = -1$, $\chi(R) = +1$ otherwise) it follows that a mechanism of this symmetry preserves the two σ_v reflection planes, removes σ_d , and distorts the square into a rhombus with C_{2v} symmetry, where the three constraint types then have the following characters under the symmetry operations:

$\mathcal{G} = C_{2v}$	E	C_2	σ_y	σ_x	Representation
$\Gamma(D_{PP})$	4	0	0	0	$A_1 + A_2 + B_1 + B_2$
$\Gamma(D_{PL})$	4	0	-2	-2	$2A_2 + B_1 + B_2$
$\Gamma(A_{LL})$	1	1	-1	-1	A_2

Summing the representations for the three constraint types gives

$$\Gamma_{\text{constraint}} = A_1 + 4A_2 + 2B_1 + 2B_2. \quad (7.7)$$

The freedoms of the points span $2(A_1 + A_2 + B_1 + B_2)$ in C_{2v} and those of the lines $2A_2 + B_1 + B_2$. Hence,

$$\Gamma_{\text{freedom}} = 2A_1 + 3A_2 + 2B_1 + 2B_2, \quad (7.8)$$

and, with $\Gamma_{\text{rigid}} = A_2 + B_1 + B_2$, the net mobility is

$$\Gamma(m) - \Gamma(s) = A_1 - A_2, \quad (7.9)$$

revealing a mechanism of A_1 symmetry, which is balanced in the scalar count by a state of self stress of A_2 symmetry. The mechanism is not blocked by the state of self-stress and is finite. The removal of the A_{LL} constraint eliminates the self-stress of A_2 symmetry without affecting the A_1 mechanism. Hence the angular constraint remains locally redundant. This reflects the well-known theorem of geometry that the two diagonals of a rhombus are always perpendicular.

The addition of a distance constraint between two diagonally opposite points in the rhombus adds an extra term A_1 to $\Gamma_{\text{constraint}}$ and hence destroys the mechanism with A_1 symmetry without changing the symmetry of the A_2 state of self-stress, to give $\Gamma(m) - \Gamma(s) = -A_2$.

7.2 3D

Non-crossing four-bar linkage in 3D We can rework the preceding example in 3D by constraining the four points to lie on a plane. The group of symmetries, D_{4h} , now includes a reflection in the plane and four half-turn rotations around σ_v and σ_d axes. There is an additional plane symmetry

element and four additional point-plane coincidence constraints. The tabular character calculation is shown below. Note the conventional reversal of labellings between σ_v and σ_d mirror lines in 2D and corresponding mirror planes in 3D (see Figures 3 and 4).

$\mathcal{G} = D_{4h}$	E	$2C_4$	C_2	$2C'_2$	$2C''_2$	i	$2S_4$	σ_h	$2\sigma_v$	$2\sigma_d$
$-\Gamma(D_{PP})$	-4	0	0	-2	0	0	0	-4	-2	0
$-\Gamma(D_{PL})$	-8	0	0	0	4	0	0	0	0	0
$-\Gamma(D_{PS})$	-4	0	0	0	2	0	0	4	0	-2
$-\Gamma(A_{LL})$	-1	1	-1	-1	1	-1	1	-1	-1	1
$-\Gamma_{\text{constraint}}$	-17	1	-1	-3	7	-1	1	-1	-3	-1
$\Gamma(P)$	12	0	0	0	-2	0	0	4	0	2
$\Gamma(L)$	8	0	0	0	-4	0	0	0	0	0
$\Gamma(S)$	3	1	-1	-1	-1	1	-1	-3	1	1
Γ_{freedom}	23	1	-1	-1	-7	1	-1	1	1	3
$-\Gamma_{\text{constraint}}$	-17	1	-1	-3	7	-1	1	-1	-3	-1
$-\Gamma_T - \Gamma_R$	-6	-2	2	2	2	0	0	0	0	0
$\Gamma(m) - \Gamma(s)$	0	0	0	-2	2	0	0	0	-2	2
$\Gamma(D_{PS}) - \Gamma_S$	1	-1	1	1	-1	-1	1	-1	-1	1
$\Gamma(D_{LL})$	1	-1	1	1	-1	-1	1	-1	-1	1

This calculation shows that $\Gamma(m) - \Gamma(s) = B_{2g} - B_{1g}$. The B_{2g} mechanism is finite as it cannot be blocked by a B_{1g} stress. The angular constraint has $\Gamma(A_{LL}) = B_{1g}$ and is locally redundant.

An alternative way to force the quadrilateral to be planar is to constrain the two lines to intersect in 3-space. This is achieved by deleting the plane and the four point-plane constraints and adding a distance-zero constraint between the two lines. As the table also shows, the characters for $\Gamma(D_{PS}) - \Gamma(S)$ and $\Gamma(D_{LL})$ are equal (irreducible representation B_{1u}).

If we now delete the D_{LL} constraint we get an additional finite mechanism with B_{1u} symmetry which takes the four points out of coplanarity into a configuration with D_{2d} symmetry where the axis of symmetry is along the line which is perpendicular to both lines (see Figure 4(iii)) for the case of a line-line distance constraint with the lines perpendicular and non-zero distance).

After restoring the line-line distance constraint, the row for $\Gamma(m) - \Gamma(s)$ in the character table has entries 0, 0, -2, 0, 2 in the columns for E , C_2 , $2C'_2$, $2S_4$ and $2\sigma_d$, respectively. This shows that $\Gamma(m) - \Gamma(s) = B_2 - B_1$ in D_{2d} symmetry and we have a finite mechanism with B_2 symmetry and a stress with B_1 symmetry. The line-line angle constraint has $\Gamma(A_{LL}) = B_1$ and is again

redundant. This reflects the geometric theorem that the diagonals of an equilateral quadrilateral are perpendicular even if the points are not coplanar and the diagonals do not intersect.

In fact all of these properties for non-crossing 4-bar mechanisms reflect an underlying rigidity property that any polygon of bars and joints in 3D, where the joints are constrained alternately to lie on a pair of orthogonal lines (which need not intersect), is dependent. For a 4-bar mechanism in the plane, this follows from the properties of an orthodiagonal quadrilateral. The extension to a $(2n)$ -bar mechanism in 3D, where the lines need not intersect, is straightforward. Our symmetry results demonstrate symmetric projections of the general result.

Examples based on the dodecahedron The following four examples are based on the regular dodecahedron, chosen as a moderately complicated three-dimensional structure of points, lines and planes. A dodecahedral configuration has 20 points representing the vertices, 12 planes representing the faces and 30 lines representing the edges. The appropriate point symmetry group of the regular Platonic dodecahedron is I_h , consisting of 120 operations based on the 60 rotations about C_5 , C_3 and C_2 axes through opposite face centres, vertices and edge midpoints, compounded with inversion symmetry to generate the 60 improper operations of the group, including 15 reflection planes.

The four examples that follow explore the consequences for mobility of changing various constraints on the geometries. Note that there is an exact cancellation between the characters for the freedoms of a line (Table 1) and those for two D_{PL0} constraints (Figure 4) for any setting in which the line passes through two distinct points (this also follows from the fact that there is a unique line through two distinct points). Hence we omit these characters from the tables.

Example (a) Consider a dodecahedron as a set of twenty points arranged on congruent planar faces with thirty edges of equal length, all in full I_h symmetry. Is an assembly of geometries with these constraints rigid or flexible? Scalar counting gives exact cancellation of 96 freedoms by 90 constraints and 6 rigid-body motions. The dodecahedron is illustrated in Figure 6(a) A full tabular calculation using all ten classes of symmetry operations of I_h to classify the symmetries of the freedoms of points and planes, together with those of the 30 constraints on point-point distances and the 60 constraints on point-plane distances gives (with $\phi = (\sqrt{5} + 1)/2$):

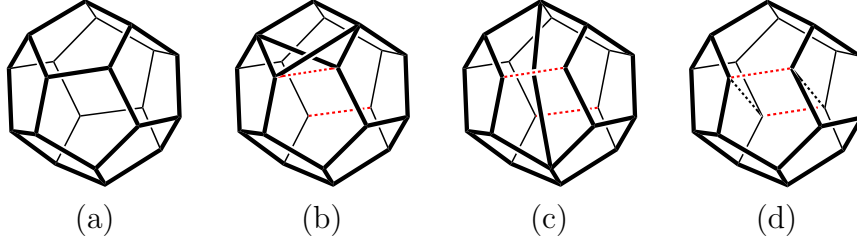


Figure 6: Constraints on a dodecahedron. In (a) all faces are planar and all edges are of the same fixed length. In the other panels, distance constraints on two opposite edges (dotted) are replaced by (b) fixed chord lengths on one face, (c) point-line distance constraints to one of the missing edges, and (d) parallel constraints on the pair of missing edges, respectively.

$\mathcal{G} = I_h$	E	$12C_5$	$12C_5^2$	$20C_3$	$15C_2$	i	$12S_{10}$	$12S_{10}^3$	$20S_6$	15σ
$\Gamma(P)$	20	0	0	2	0	0	0	0	0	4
$\times \Gamma_T$	3	ϕ	$-\phi^{-1}$	0	0	-1	-3	ϕ^{-1}	$-\phi$	1
$\Gamma(P) \times \Gamma_T$	60	0	0	0	0	0	0	0	0	4
$\Gamma(S)$	12	2	2	0	0	0	0	0	0	4
$-\Gamma(S) \times \Gamma_\epsilon$	-12	-2	-2	0	0	0	0	0	0	4
$+\Gamma(S) \times \Gamma_R$	36	2ϕ	$-2\phi^{-1}$	0	0	0	0	0	0	-4
Γ_{freedom}	96	2ϕ	$-2\phi^{-1}$	0	0	0	0	0	0	4
$-\Gamma(D_{PP})$	-30	0	0	0	-2	0	0	0	0	-4
$-\Gamma(D_{PS})$	-60	0	0	0	0	0	0	0	0	-4
$-(\Gamma_T + \Gamma_R)$	-6	-2ϕ	$2\phi^{-1}$	0	2	0	0	0	0	0
$\Gamma(m) - \Gamma(s)$	0	0	0	0	0	0	0	0	0	0

Note the exact cancellation of intrinsic point freedoms and point-plane constraints that arises from the symmetry equivalence in this case between $\Gamma(D_{PS})$ and $\Gamma(P) \times \Gamma_T$. This also follows from the fact that there is a unique intersection point for three pairwise non-parallel planes. The final result that $\Gamma(m) - \Gamma(s)$ spans the null representation implies that the system is either rigid or has mechanisms masked by equisymmetric and states of self stress. Numerical computation of the rank of the Jacobian matrix of the corresponding constraint equations confirms the structure as rigid.

Example (b) In the configuration illustrated in Figure 6(b), two distance constraints on antipodal edges have been replaced by chordal distance constraints on a face, preserving the isostatic property. There are two distinct ways to place the chords to be compatible with a reduced point-group

symmetry of C_s , where only the columns for the identity E and a single mirror plane σ are retained from the earlier tabular calculation. The representations of freedoms and rigid body motions from the table for the icosahedrally symmetric configuration (a) reduce to $\{\chi(E), \chi(\sigma)\} = \{96, 8\}$ (freedoms), $\{3, 0\}$ ($\Gamma_T + \Gamma_R$), and the constraint representation $\{90, 8\}$ is changed by deletion of two edges ($\{-2, -2\}$) and addition of chords that exchange under reflection ($\{+2, 0\}$). Hence, the net mobility representation becomes $\{0, 2\} = \{1, 1\} - \{1, -1\}$, corresponding to reducible representation $\Gamma(m) - \Gamma(s) = A' - A''$. The prediction is of a mirror-symmetric breathing flex and an antisymmetric state of self stress. Numerical computation of the rank of the Jacobian matrix of the corresponding constraint equations confirms there are no additional states of stress and hence that the flex is indeed continuous (Kangwai and Guest, 1999; Guest and Fowler, 2007).

Example (c) In the configuration illustrated in Figure 6(c), two edge distance constraints have been replaced by a total of two point-line distance constraints, to give a configuration with point group C_{2v} . We take the mirror planes preserving and exchanging the point-line constraints as σ_x and σ_y , respectively. The calculation is then:

$\mathcal{G} = C_{2v}$	E	C_2	σ_y	σ_x
Γ_{freedom}	96	0	8	8
$-\Gamma_{\text{constraint}}$	-90	0	-6	-8
$-(\Gamma_T + \Gamma_R)$	-6	2	0	0
$\Gamma(m) - \Gamma(s) =$	0	2	2	0

and, as a reducible representation, $\Gamma(m) - \Gamma(s) = \{1, 1, 1, 1\} - \{1, -1, -1, 1\} = A_1 - B_1$, indicating a fully symmetric mechanism and a state of self-stress with the symmetry of a tangential vector parallel to the missing edges. Again, detection of a totally symmetric mechanism implies that the mechanism could be finite. Numerical evaluation of the rank of the rigidity matrix confirms that there are no blocking states of self-stress undetected by symmetry.

Example (d) In the final variation of the dodecahedron constraints from (a), the distance constraints on a pair of opposite edges are removed, but the point-to-point vectors corresponding to the two former edges are constrained to be parallel, i.e. with a constraint of type $A_{LL\parallel}$. This configuration is shown in maximum symmetry (point group D_{2h}) in Figure 6(d). The character table (Table 4) for the D_{2h} subgroup of I_h in the setting used in Figure 4 lists the behaviour of the 8 irreducible representations under the 8 classes of symmetry operations in this Abelian group.

$\mathcal{G} = D_{2h}$	E	$C_2(z)$	$C_2(y)$	$C_2(x)$	i	σ_z	σ_y	σ_x
A_g	1	1	1	1	1	1	1	1
B_{1g}	1	1	-1	-1	1	1	-1	-1
B_{2g}	1	-1	1	-1	1	-1	1	-1
B_{3g}	1	-1	-1	1	1	-1	-1	1
A_u	1	1	1	1	-1	-1	-1	-1
B_{1u}	1	1	-1	-1	-1	-1	1	1
B_{2u}	1	-1	1	-1	-1	1	-1	1
B_{3u}	1	-1	-1	1	-1	1	1	-1

Table 4: Character table for point group D_{2h}

We calculate the mobility of this configuration by difference from the null symmetry found in example (a). Removal of two edge constraints adds freedoms spanning $\Delta\Gamma_{\text{freedom}}$, countered by imposition of the two-dimensional parallelism constraints spanning $\Delta\Gamma_{\text{constraint}}$, where:

$\mathcal{G} = D_{2h}$	E	$C_2(z)$	$C_2(y)$	$C_2(x)$	i	σ_z	σ_y	σ_x	
$\Delta\Gamma_{\text{freedom}}$	2	0	2	0	0	2	0	2	$= A_g + B_{2u}$
$\Delta\Gamma_{\text{constraint}}$	2	0	0	2	-2	0	0	-2	$= A_u + B_{3u}$

indicating that the count of $m - s = 0$ in this case conceals two net freedoms accompanied by states of self stress of orthogonal symmetries. The mobility space includes a non-totally symmetric motion that would allow distortion from D_{2h} to C_{2v} symmetry. As the states of self-stress would remain non-totally symmetric in this lower group there is no reason based on symmetry to suppose that the motions would be blocked, and indeed numerical calculations confirm the presence of a two-dimensional space of continuous flexes for this configuration. Once again, useful information about freedoms has been revealed by extending counting with symmetry.

(e) An example based on the cube Consider a cube as a set of eight points arranged on six congruent planar faces with twelve edges of equal length, in full O_h symmetry. Scalar counting gives exact cancellation of 42 freedoms by 36 constraints and 6 rigid-body motions. A full tabular calculation, using all ten classes of symmetry operations of O_h to classify the symmetries of the freedoms of points and planes, together with those of the 12 constraints on point-point distances and the 24 on point-plane distances, gives:

$\mathcal{G} = O_h$	E	$8C_3$	$6C_2$	$6C_4$	$3C_2$	i	$6S_4$	$8S_6$	$3\sigma_h$	$6\sigma_d$
$\Gamma(P)$	8	2	0	0	0	0	0	0	0	4
Γ_T	3	0	-1	1	-1	-3	-1	0	1	1
$\Gamma(P) \times \Gamma_T$	24	0	0	0	0	0	0	0	0	4
$\Gamma(S)$	6	0	0	2	2	0	0	0	4	2
$\Gamma(S) \times \Gamma_T$	18	0	0	2	-2	0	0	0	4	2
Γ_{freedom}	42	0	0	2	-2	0	0	0	4	6
$-\Gamma(D_{PP})$	-12	0	-2	0	0	0	0	0	-4	-2
$-\Gamma(D_{PS})$	-24	0	0	0	0	0	0	0	0	-4
$-(\Gamma_T + \Gamma_R)$	-6	0	2	-2	2	0	0	0	0	0
$\Gamma(m) - \Gamma(s)$	0	0	0	0	0	0	0	0	0	0

where we have used (4.10) to express the face freedoms of the polyhedron as $\Gamma(S) \times \Gamma_T$. The result in the final line is that $\Gamma(m) - \Gamma(s)$ spans the null representation, which implies that the configuration is either rigid or has mechanisms masked by equisymmetric states of self-stress. The latter is in fact the case, as it is straightforward to show (see below) that this configuration has a set of three symmetry-equivalent finite mechanisms in which pairs of opposite faces flex into congruent rhombi. In the initial high symmetry of the cube, this set corresponds to the representation T_{2g} in O_h , with pure distortion along any one of the three orthogonal modes leading to D_{2h} symmetry. An arbitrary mixture of all three modes reduces the point group to C_i , preserving only inversion symmetry.

The space of finite distortions can be characterised as follows. Label the points p_1, p_2, p_3, p_4 in cyclic order on one face and corresponding points p_5, p_6, p_7, p_8 on the opposite face, hence with pairs $\{p_i, p_{9-i}\}$ related by inversion. Assume all edges have length 1. Let $\hat{b}(\theta, \phi) = \sin \theta (\cos \phi \hat{x} + \sin \phi \hat{y}) + \cos \phi \hat{z}$ be a unit vector, and $\hat{a}(\chi) = \cos \chi \hat{x} + \sin \chi \hat{y}$ be a unit vector in the xy plane. Let $p_1 = (0, 0, 0)$, $p_2 = (1, 0, 0)$, $p_3 = p_2 + \hat{a}(\chi)$, $p_4 = p_1 + \hat{a}(\chi)$, $p_5 = p_1 + \hat{b}(\theta, \phi)$, $p_6 = p_2 + \hat{b}(\theta, \phi)$, $p_7 = p_3 + \hat{b}(\theta, \phi)$, $p_8 = p_4 + \hat{b}(\theta, \phi)$. Then $|p_{12}| = |p_{23}| = |p_{34}| = |p_{14}| = |p_{56}| = |p_{67}| = |p_{78}| = |p_{58}| = 1$. Points $\{p_1, p_2, p_3, p_4\}$ are coplanar because p_{12} is parallel to p_{34} . Similarly, sets $\{p_5, p_6, p_7, p_8\}$, $\{p_1, p_4, p_5, p_8\}$, $\{p_2, p_3, p_6, p_7\}$, $\{p_1, p_2, p_5, p_6\}$, $\{p_3, p_4, p_7, p_8\}$ are each coplanar. The three infinitesimal flexes that correspond to changes in χ , θ and ϕ are independent unless θ or ϕ are 0 or π . Hence, there are three independent finite mechanisms except at special points.

Figure 7 illustrates one realisation of the set of mechanisms and their matching states of self-stress for the floppy cube. The degenerate irreducible representation T_{2g} is spanned by the set of cartesian spherical harmonic functions $\{xy, yz, zx\}$, and these can be used to project out a set of three indepen-

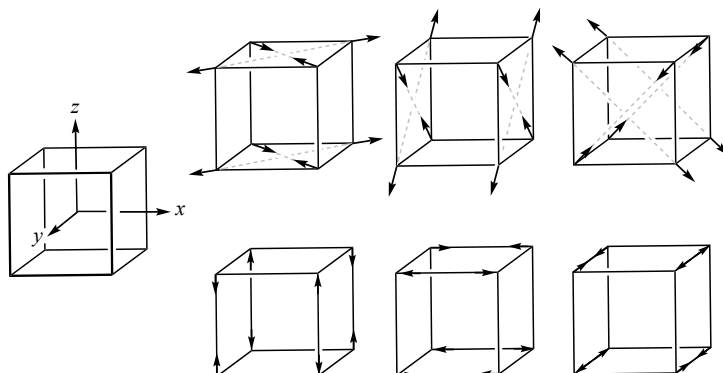


Figure 7: Equisymmetric flexes and states of self-stress for the ‘floppy cube’ (with fixed edge lengths and planar faces). In the axis system defined on the left, sets of independent flexes (top) and states of self-stress (bottom) transform as the coordinate products $\{xy, yz, zx\}$. For the flexes, arrows indicate the direction of the initial displacement from the high-symmetry configuration; for the states of self-stress, inward/outward-pointing arrows indicate tensile/compressive force.

dent flexes and corresponding states of self-stress. Flexes have displacements in the planes of the maxima in the cartesian function; thus four cube faces rotate and two flex to make a rhombus. Each pattern of stresses involves four D_{PP} constraints on the edges normal to the nominated cartesian plane, with an alternating cyclic pattern $(+s, -s, +s, -s)$.

Point groups O_h , D_{2h} , D_{3d} , C_{2h} and C_i are accessible in this distortion space (figure 8). (See Guest and Fowler (2007), and also Jotham and Kettle (1971) where the same descent in symmetry is discussed for a problem in chemistry related to Jahn-Teller distortion in octahedral complexes.)

8 Mobility predictions for convex polyhedra

Simple counting of freedoms and constraints gives only the net mobility $m - s$ and no conditions on the individual values of m and s . The symmetry-extended approach gives, in effect, a further set of necessary conditions on m and s , through determination of the difference $\Gamma(m) - \Gamma(s)$, but again is not guaranteed to give full information on the separate representations $\Gamma(m)$ and $\Gamma(s)$. Symmetry often gives some added information through the pattern of signs in the reducible representation, giving partial but unambiguous contributions to $\Gamma(m)$ and $\Gamma(s)$. To take a concrete example, a count $m - s = 0$

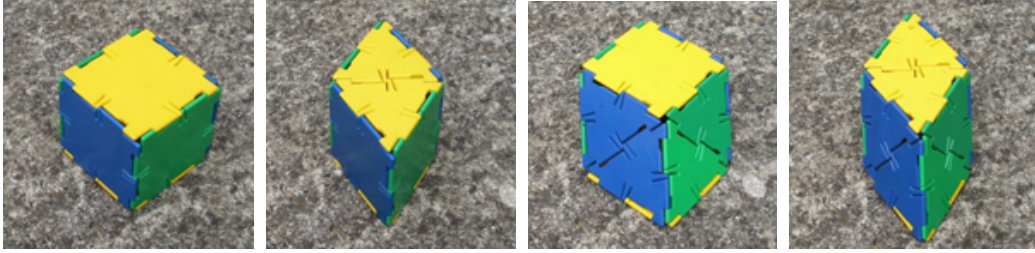


Figure 8: Symmetries accessible in the T_{2g} space of mechanisms of a cube with fixed edge lengths and planar faces, illustrated with Polydron models. (Models consist of square plates and planar rhombi constructed from pairs of equilateral triangular plates.) The point groups are (left to right) O_h , D_{2h} , C_{2h} , D_{3d} , with respectively 6, 4, 2, and 0 square, and 0, 2, 4, and 6 rhomboidal faces.

shows that m and s are equal but not that they vanish individually. By the same token, if computation leads to the conclusion that $\Gamma(m) - \Gamma(s)$ is the null representation, we know only that $m = s$ and that the sets of mechanisms and states of self-stress are equisymmetric.

3D examples (a) to (d) include two cases where a cubic polyhedron under the sole constraints of fixed edge lengths and planarity of faces turns out to have the null representation for $\Gamma(m) - \Gamma(s)$. We can generalise this result to show that the mobility of *any* convex polyhedron under these constraints will span the null representation, $\Gamma(m) - \Gamma(s) = 0$.

The proof follows a method used for deriving the symmetry extension of the Euler theorem (Ceulemans and Fowler, 1991). Let $\Gamma(F)$, $\Gamma(E)$ and $\Gamma(V)$ be the reducible representations for the permutations induced by symmetry elements of the group \mathcal{G} on the sets of vertices, edges and faces of a polyhedron, with characters $\chi_F(R)$, $\chi_E(R)$ and $\chi_V(R)$ equal to the numbers of components of each type that are unshifted under operation $R \in \mathcal{G}$.

The case of the identity operation, $R = E$, is that of pure scalar counting. Suppose the polyhedron has f faces, e edges, and v vertices, and let face i have n_i vertices. There are n_i constraints of type D_{PS} on the plane of face i and n_i edges on face i . We have $\sum_i n_i = 2e$, as each edge is on two faces. Hence, we have in total $3(f + v)$ freedoms, $2e$ constraints D_{PS} and e constraints D_{PP} for our polyhedron with fixed-length edges and planar faces, and thus

$$F - C - 6 = 3(f + v - e - 2) = 0, \quad (8.1)$$

by Euler's theorem.

Next, consider a rotation through a non-zero angle ϕ , i.e. the proper

rotation C_ϕ . We have $\Gamma_{\text{freedom}} = (\Gamma(P) + \Gamma(S)) \times \Gamma_T$. The axis of rotation must pass through two structural elements of the polyhedron (vertex + vertex, vertex + edge midpoint, vertex + face centre, ..., face centre + face centre). It may pass through an edge centre if $\phi = \pi$. Let the number of faces, edges and vertices intersected by a given C_ϕ axis be f_ϕ , e_ϕ and v_ϕ , respectively, with $f_\phi + e_\phi + v_\phi = 2$, and let the character of the rigid-body translations be $\chi_T(C_\phi)$ (with explicit formula $\chi_T(C_\phi) = 1 + 2 \cos \phi$ and hence $\chi_T(C_\phi) = -1$ for $\phi = \pi$). Then, for the character of the freedoms we have $\chi_{\text{freedom}}(C_\phi) = (f_\phi + v_\phi)\chi_T(C_\phi)$. For the edge constraints we have $\chi_{PP}(C_\phi) = e_\phi = -e_\phi\chi_T(C_\phi)$ as either $\phi = \pi$ or $e_\phi = 0$, or both. For the planarity constraints we have $\chi_{PS} = 0$, as no vertex is at the centre of a face. Rigid-body motions give $\chi_T(C_\phi) + \chi_R(C_\phi) = 2\chi_T(C_\phi)$. Hence, in total we have

$$\chi_{m-s}(C_\phi) = (f_\phi + v_\phi)\chi_T(C_\phi) + e_\phi \times \chi_T(C_\phi) - 2\chi_T(C_\phi) = 0. \quad (8.2)$$

All faces, edges and vertices are shifted by inversion and rotation-reflections, so it remains only to consider a pure reflection, $R = \sigma$. A mirror plane intersects the shell in a loop of linked intersection elements of at most four types (Ceulemans and Fowler, 1991). These are shown as (i) to (iv) in Figure 9. Counting contributions, using half weighting for edges or vertices shared between two intersected elements, gives

Character	(i)	(ii)	(iii)	(iv)
$\chi_S(\sigma)$	1	1	1	0
$\chi_P(\sigma)$	0	$\frac{1}{2}$	$\frac{1}{2} + \frac{1}{2}$	$\frac{1}{2} + \frac{1}{2}$
$-\chi_{DPP}(\sigma)$	$-(\frac{1}{2} + \frac{1}{2})$	$-\frac{1}{2}$	0	-1
$-\chi_{DPS}(\sigma)$	0	-1	-2	0
$-\chi_T(\sigma) - \chi_R(\sigma)$	0	0	0	0
$\chi_{m-s}(\sigma)$	0	0	0	0

which shows that $\chi_{m-s}(\sigma)$ sums to zero over the whole loop for every reflection plane. Hence, $\Gamma(m) - \Gamma(s) = 0$ for all polyhedra subject only to full edge-length and face-planarity constraints. \square

As we have seen, vanishing of the mobility representation does not exclude the possibility of undetected mechanisms. The example of the cube suggests an infinite family of polyhedra with such mechanisms: any polyhedron constructed by *extrusion of a polygon*, i.e. formed by joining corresponding vertices of two parallel congruent copies of polygons, will have all those mechanisms that derive from in-phase combinations of the 2D mechanisms of the parallel polygons (if the polygons are of size greater than 3). Prisms form a subclass of extruded polyhedra. For the cube, the extrusion can be considered to have happened in any one of three independent directions, hence the threefold nature of the mechanism.

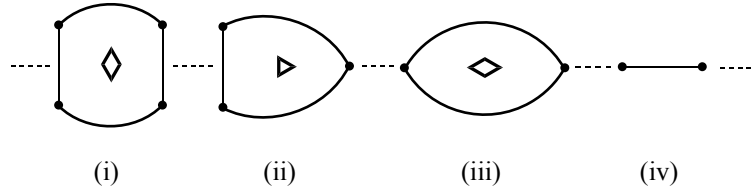


Figure 9: Intersection of a reflection plane with structural elements of a polyhedron (Ceulemans and Fowler, 1991). See text for details of the calculation of their contributions to the mobility representation.

9 A note on freedoms of a cubic polyhedral cage

The general symmetry-extended treatment can often be taken further in specific situations. One such specialisation, which is of interest in several contexts, from CAD to structural mechanics and molecular force fields in physical chemistry, is based on the family of *cubic polyhedral cages*. In a CAD context, a polyhedron can be considered as an assemblage of point, line and plane geometries. The polyhedral cages have rings of vertices and edges in place of solid faces, and these rings are not necessarily planar. Here we concentrate on the freedoms of edges and vertices. From (4.1), (4.3), and (4.9), replacing P and L by v and e , respectively, these are:

$$\text{vertices:} \quad \Gamma(v) \times \Gamma_{\text{T}}, \quad (9.1)$$

$$\text{edges:} \quad \Gamma(e) \times (\Gamma_{\text{T}} + \Gamma_{\text{R}}) - \Gamma_{\parallel}(e) \times (\Gamma_0 + \Gamma_{\epsilon}), \quad (9.2)$$

For the object as a whole, rigid-body motions are accounted for by subtraction of one copy of $(\Gamma_{\text{T}} + \Gamma_{\text{R}})$.

The sets of freedoms are not independent for a polyhedral object, as the Euler theorem and its symmetry-adapted counterpart apply, with significant consequences, as illustrated here for cubic polyhedra. We can give physical interpretations to the freedom equations and their differences. One such difference is relevant to the construction of force fields for cubic polyhedral molecular cages.

A set of edges, given full line freedoms, will simply drift apart. The representation $\Gamma_{\text{freedom}}(e)$ must be reduced by some constraint Γ_{ev} to produce $\Gamma(v) \times \Gamma_{\text{T}}$, the mechanical freedoms of the polyhedral cage. The constraint is that at each vertex of a cubic polyhedron the three incident edges must have a common intersection and therefore must satisfy three pairwise intersection constraints of type D_{LL0} .

We can show that these constraints correspond to a *rotational* triple at each vertex, and hence span

$$\Gamma_{ev} = \Gamma_{\text{freedom}}(e) - \Gamma_{\text{freedom}}(v) = \Gamma(v) \times \Gamma_R = \Gamma(v) \times \Gamma_T \times \Gamma_\epsilon. \quad (9.3)$$

The proof is straightforward. Expansion of Γ_{ev} using (4.3) and (4.1) gives

$$\Gamma_{ev} = \Gamma(e) \times (\Gamma_T + \Gamma_R) - \Gamma_{\parallel}(e) \times (\Gamma_0 + \Gamma_\epsilon) - \Gamma(v) \times \Gamma_T, \quad (9.4)$$

and this can be simplified using the identities

$$\Gamma(e) \times \Gamma_T = \Gamma(e) + \Gamma_{\parallel}(e) + \Gamma_{\perp}(e), \quad (9.5)$$

$$\Gamma_{\parallel}(e) = \Gamma_{\perp}(e) \times \Gamma_\epsilon, \quad (9.6)$$

and a specific consequence for cubic polyhedra of the symmetry-extended Euler theorem (Ceulemans and Fowler, 1991),

$$\Gamma(v) \times \Gamma_T = \Gamma(e) + \Gamma_{\parallel}(e), \quad (9.7)$$

to give Γ_{ev} as a function of edge representations, which collapses down to

$$\Gamma_{ev} = \Gamma(e) \times \Gamma_\epsilon + \Gamma_{\perp}(e) = \Gamma(v) \times \Gamma_T \times \Gamma_\epsilon = \Gamma(v) \times \Gamma_R. \quad (9.8)$$

Hence, (9.3) is proved. \square

The combination $\Gamma(v) \times \Gamma_R$ also arises in other contexts. For example, in Guest et al. (2018) it appears as the symmetry spanned by extra states of self-stress in a panel-hinge description of the net mobility of a fully triangulated polyhedron (‘extra’ compared to the isostatic bar-and-joint model). As also in the present application, the key point is that hinge lines (edges) associated with panels (or faces) around each polyhedral vertex meet at that common vertex.

The identity (9.7) expresses the under-appreciated fact that the vibrational motions of a cubic polyhedral molecular framework can be expressed as a combination of bond stretches and ‘bond slides’ only, giving a basis for a novel type of force field for polyhedral cage molecules (Ceulemans et al., 2001).

10 Conclusions

A general symmetry extension of counting rules for CAD systems has been derived. Symmetry extensions of counting arguments are useful in many specific cases for deciding local redundancy of constraints, residual freedoms of

the geometries and the quadratic solvability of constraint equations. They also lead to general results for families of CAD systems, including, surprisingly, some where we can show that it is impossible to detect mechanisms by point-group-symmetry counting alone.

We finish with two further observations about the scope for the use of symmetry in CAD, as discussed here. The first is an intrinsic limitation of all symmetry-based treatments. Our premise for introducing symmetry was that a pure counting argument gives a necessary but not sufficient criterion for establishing residual freedoms in a CAD drawing. Consideration of symmetry gives a hierarchy of necessary but possibly still not sufficient criteria. Hidden flexes/mechanisms may be revealed, but sometimes cancellation hides further layers of detail, as for example when there is a geometric invariant of the kind found for the Stewart platform.

The second observation is more positive, in that although we have considered only point-group symmetry and rather simple objects here, there are further possibilities for symmetry-based explanations. The choice of objects can be made richer: spheres for points, cylinders for lines, and laminae for planes. More exotic surfaces can be considered, and the notion of symmetry can also be widened, to include other conserved invariants that generate an abstract group and hence open up possibilities for more symmetry-extended counting arguments (Olver, 1999).

11 Acknowledgements

The authors thank the referees for a number of useful comments on presentation for the CAD audience of the ideas in this paper.

References

- Altmann, S. L. and Herzig, P. (1994). *Point-Group Theory Tables*. Clarendon Press, Oxford.
- Atkins, P. W., Child, M. S., and Phillips, C. S. G. (1970). *Tables for Group Theory*. Oxford University Press.
- Barton, M., Shragai, N., and Elber, G. (2009). Kinematic simulation of planar and spatial mechanisms using a polynomial constraints solver. *Computer-Aided Design and Applications*, 6(1):115–123.
- Bishop, D. M. (1973). *Group Theory and Chemistry*. Clarendon Press, Oxford.

- Bouma, W., Fudos, I., Hoffmann, C., Cai, J., and Paige, R. (1995). Geometric Constraint Solver. *Computer-aided Design.*, 27(6):487–501.
- Calladine, C. R. (1978). Buckminster Fuller’s “Tensegrity” structures and Clerk Maxwell’s rules for the construction of stiff frames. *International Journal of Solids and Structures*, 14:161–172.
- Ceulemans, A. and Fowler, P. W. (1991). Extension of Euler’s theorem to the symmetry properties of polyhedra. *Nature*, 353:52–54.
- Ceulemans, A., Titeca, B. C., Chibotaru, L. F., Vos, I., and Fowler, P. W. (2001). Complete bond force fields for trivalent and deltahedral cages: group theory and applications to cubane, closo-dodecaborane and buckminsterfullerene. *Journal of Physical Chemistry A*, 105:8284–8295.
- Fowler, P. W. and Guest, S. D. (2000). A symmetry extension of Maxwell’s rule for rigidity of frames. *International Journal of Solids and Structures*, 37:1793–1804.
- Fowler, P. W. and Guest, S. D. (2005). A symmetry analysis of mechanisms in rotating rings of tetrahedra. *Proceedings of the Royal Society: Mathematical, Physical & Engineering Sciences*, 461:1829–1846.
- Fowler, P. W. and Quinn, C. M. (1986). σ , π and δ representations of the molecular point groups. *Theoretica Chimica Acta*, 70(5):333–350.
- Griffith, J. S. (2009). *The Theory of Transition-Metal Ions*. Cambridge University Press.
- Guest, S. D. and Fowler, P. W. (2005). A symmetry-extended mobility rule. *Mechanism and Machine Theory*, 40:1002–1014.
- Guest, S. D. and Fowler, P. W. (2007). Symmetry conditions and finite mechanisms. *Journal of Mechanics of Materials and Structures*, 2(2):293–301.
- Guest, S. D., Fowler, P. W., and Schulze, B. (2018). Mobility of symmetric block-and-hole polyhedra. *International Journal of Solids and Structures*, 150:40–51.
- Guest, S. D., Schulze, B., and Whiteley, W. J. (2010). When is a body-bar structure isostatic? *International Journal of Solids and Structures*, 47:2745–2754.

- Jackson, B. and Owen, J. C. (2016). A characterisation of the generic rigidity of 2-dimensional point-line frameworks. *Journal of Combinatorial Theory, Series B*, 119:96–121.
- Jackson, B. and Owen, J. C. (2019). Radically solvable graphs. *Journal of Combinatorial Theory, Series B*, 136:135–153.
- Jotham, R. W. and Kettle, S. F. A. (1971). Geometrical consequences of the Jahn-Teller effect. *Inorganica Chimica Acta*, 5:183–187.
- Kangwai, R. D. and Guest, S. D. (1999). Detection of finite mechanisms in symmetric structures. *International Journal of Solids and Structures*, 36(36):5507–5527.
- Kim, K., Lee, J. Y., and Kim, K. (1998). A 2-D geometric constraint solver using dof-based graph reduction. *Computer-aided Design.*, 30(11):883–896.
- Klein, F. (1870). Zur theorie der liniencomplexe des ersten und zweiten grades. *Math. Ann.*, 2:198–226.
- Maxwell, J. C. (1864). On the calculation of the equilibrium and stiffness of frames. *Philosophical Magazine.*, 27:294–299.
- Müller, A. (2016). Recursive higher-order constraints for linkages with lower kinematic pairs. *Mechanism and Machine Theory*, 100:33–43.
- Nawratil, G. (2013). Types of self-motions of planar Stewart–Gough platforms. *Meccanica*, 48:1177–1190.
- Olver, P. J. (1999). *Equivalence, Invariants and Symmetry*. London Mathematical Society Lecture Notes, Cambridge University Press.
- Owen, J. C. (1991). Algebraic solution for geometry from dimensional constraints. In *Proceedings of the First ACM Symposium on Solid Modeling Foundations and CAD/CAM Applications*, SMA '91, pages 397–407, New York, NY, USA. ACM.
- Owen, J. C. and Power, S. C. (2006). The non-solvability by radicals of generic 3-connected planar Laman graphs. *Transactions of the American Mathematical Society*, 359:2269–2303.
- Owen, J. C. and Power, S. C. (2010). Framework symmetry and rigidity. *International Journal of Computational Geometry and Applications*, 20:723–750.

- Plücker, J. (1865a). I. on a new geometry of space. *Proceedings of the Royal Society of London*, 14:53–58.
- Plücker, J. (1865b). Xvii. on a new geometry of space. *Philosophical Transactions of the Royal Society of London*, 155:725–791.
- Quinn, C. M., McKiernan, J. G., and Redmond, D. B. (1984). Mollweide projections and symmetries on the spherical shell. *Journal of Chemical Education*, 61:569–571 and 572–579.
- Schulze, B. (2010). Symmetry as a sufficient condition for a finite flex. *SIAM Journal on Discrete Mathematics*, 24(4):1291–1312.
- Sitharam, M., St. John, A., and Sidman, J., editors (2019). *Handbook of Geometric Constraint Systems*. CRC Press.
- Spivak, M. (1965). *Calculus on manifolds. A modern approach to classical theorems of advanced calculus*. W. A. Benjamin, Inc., New York-Amsterdam.